ELSEVIER

Quaternary Science Reviews 24 (2005) 1969–1988

QSR

Sea-level change in the Mediterranean Sea since the LGM: model predictions for tectonically stable areas

Kurt Lambeck*, Anthony Purcell

Research School of Earth Sciences, Australian National University, Canberra ACT 0200, Australia

Received 17 March 2004; accepted 22 June 2004

Abstract

Sea-level change in the Mediterranean Sea during glacial cycles is determined by the temporally variable eustatic change and by the spatially variable glacio-hydro-isostatic response of the earth and ocean to the growth and decay of ice sheets. Superimposed upon this are the relative changes from any vertical tectonic movement of the land. For sites that are either tectonically stable or where the magnitude of tectonic uplift is known, comparisons of observed change with predictions of the glacio-hydro-eustatic signals provide constraints on the earth–ice parameters used. The resulting predictive models can then be used to interpolate sea-level change and shoreline migration between the spatially and temporally limited observational data set. Whether such parameters reflect the true properties of the mantle and ice sheets depends on whether an effective separation has been achieved from the inversion of the observational data set. This paper explores this issue and demonstrates that observations from certain regions in the Mediterranean are particularly important in effecting the separation. This is supported by a trial analysis of a small observation data set from sites that exhibit some of the desirable features of an ideal data set. Basin-wide predictions of sea-level change, palaeo-water depth and shoreline locations based on these analyses are presented for selected epochs.

1. Introduction

Sea level is defined by the position of the sea surface relative to the adjacent land and sea-level change is a measure of the relative shift in position of these two surfaces. A principal process contributing to sea-level change on glacial time scales is the exchange of water between the continental ice sheets and the oceans, upon which may be superimposed vertical land movements driven by active tectonic processes. The growth and decay of the ice sheets change the ocean volume, deform the ocean basins and their margins, and modify the gravitational field, or geoid, of the planet. All three effects modify sea level. The deformational and gravitational effects are spatially variable, functions largely of the distance from the ice sheets, but they are predictable if the growth and decay history of the continental ice is known. In contrast, the changes wrought by tectonic processes, tend to be less predictable, of shorter wavelength and more episodic than the glacially-driven change. When combined, the two contributions result in a complex spatial and temporal pattern of sea-level change. On longer time scales, of order $>10^6$ years, geological processes may become dominant in affecting sea level, such as plate-tectonic-driven modification of ocean-basin geometry. On shorter time scales, of years and decades and for which it has been instrumentally monitored, oceanographic and climatic forcing (including thermal expansion) of the ocean surface may become important.

The Mediterranean basin has experienced major sea-level change during glacial cycles, evidence for which occurs in both the geological and archaeological records, of decreasing resolution with time, throughout the last glacial cycle. The analysis of this information from across the region can provide insights into the

*Corresponding author. Tel.: +61 2 6125 5161; fax: +61 2 6125 5443.
E-mail address: kurt.lambeck@anu.edu.au (K. Lambeck).

0277-3791/$ - see front matter © 2005 Elsevier Ltd. All rights reserved.
doi:10.1016/j.quascirev.2004.06.025

physical properties of the solid planet, primarily the mantle viscosity, and into the changes in global ice volume through time. If the rheological and ice dependence can be established, predictive models for glacially-driven sea-level change can then be developed and used as reference for estimating vertical rates and scales of surface tectonic processes or for predicting shoreline migrations.

The Mediterranean margins and islands have provided a fruitful area for such studies for a number of reasons. First, because the area is a small tidal-range environment, the observational evidence can often be related precisely to mean sea level. Second, there is a wide range of geological and archaeological evidence available from most of the region. While this data remains inadequate to construct a purely empirical model for sea-level change that has predictive capabilities across the region, it does provide a significant database for testing and calibrating the quantitative models of change during a glacial cycle. The Mediterranean region is particularly useful in that older interglacial shorelines are preserved in many locations so that it becomes possible to examine whether changes in tectonic rates have occurred on time scales from years to $\sim 10^5$ years. Third, there are a number of active tectonic processes whose understanding would be considerably aided if rates of vertical movement can be measured over a range of time scales of 10^0–10^5 years. Finally, once successful models for sea-level change have been developed, it is also possible to predict past and future shoreline migrations and to address, for example, questions about the functions of coastal archaeological structures or help in exploring the submarine environment for past sites of human activity.

In this paper, we are concerned with the eustatic and glacio-hydro-isostatic contributions to sea level across the Mediterranean basin, with a focus on change since the end of the last glaciation about 20,000 years ago. Over the past decade a number of studies have been undertaken to establish regional predictive models (Lambeck, 1996; Lambeck and Bard, 2000; Sivan et al., 2001, 2004; Lambeck et al., 2004a, b). Here, we attempt a basin-wide study that integrates some of these results. Emphasis is on demonstrating the nature of the spatially and temporally variable level across the Mediterranean basin and on assessing how this variability can be exploited to establish optimum parameters for modeling sea-level change through time. Preliminary comparisons with observational evidence are made to test the essential correctness of the model. In a follow-up paper, this model will be compared more rigorously with observational evidence from across the region, with the objective of estimating improved rheological parameters and with providing an improved reference surface for measuring rates of tectonic uplift and subsidence.

2. Theory and model requirements

2.1. Theory

The theory for glacio-hydro-isostasy used here has been developed over a period of years by Nakiboglu et al. (1983), Nakada and Lambeck (1987), Johnston (1993, 1995), Lambeck and Johnston (1998), and Lambeck et al. (2003), with successive models representing improvements in theory, computational methods, and model-parameter estimation. There has been some discussion on aspects of the theory that we use concerning the distribution of the glacial melt water into the deformable ocean basins (Peltier, 2002) but according to Mitrovica and Milne (2003), the theory used here represents, along with that of Milne (1998), the most complete and rigorous available (see also Mitrovica, 2003).

We do not discuss the theory in detail since this is given in the above references. Instead, we express relative sea-level change $\Delta\zeta_{\rm rsl}(\varphi, t)$ schematically as

$$\Delta\zeta_{\rm rsl}(\varphi, t) = \Delta\zeta_{\rm esl}(t) + \Delta\zeta_{\rm I}(\varphi, t) + \Delta\zeta_{\rm T}(\varphi, t) \tag{1a}$$

with

$$\Delta\zeta_{\rm I}(\varphi, t) = \Delta\zeta_{\rm I\text{-}g}(\varphi, t) + \Delta\zeta_{\rm I\text{-}h}(\varphi, t) \tag{1b}$$

where $\Delta\zeta_{\rm rsl}(\varphi, t)$ represents the change at location φ of the sea surface relative to land at time t compared to its present position at time $t_{\rm P}$. The first term on the right-hand side of Eq. (1a) represents the ice-volume equivalent sea-level contribution (esl), the second term, $\Delta\zeta_{\rm I}(\varphi, t)$, is the isostatic contribution, and the last term is a tectonic contribution for tectonically active areas. The isostatic term is schematically divided into two contributions: the glacio-isostatic part $\Delta\zeta_{\rm I\text{-}g}(\varphi, t)$, and the hydro-isostatic part $\Delta\zeta_{\rm I\text{-}h}(\varphi, t)$.

The ice-volume equivalent term is defined as

$$\Delta\zeta_{\rm esl}(t) = -\frac{\rho_{\rm i}}{\rho_{\rm o}} \int_t \frac{1}{A_{\rm o}(t)} \frac{{\rm d}V_{\rm i}}{{\rm d}t}\, {\rm d}t. \tag{2}$$

$V_{\rm i}$ is the ice volume at time t, $A_{\rm o}(t)$ is the ocean surface area at time t, and $\rho_{\rm i}$, $\rho_{\rm o}$ are the average densities of ice and ocean water. In the absence of any other factors that lead to changes in ocean volume, the ice-volume equivalent sea-level is equal to eustatic sea level. In our formulation, the ice load is evaluated from the integral over the ice mass on the continents and grounded on continental shelves. The water load is then defined by the shoreline at the epoch in question and by the grounding line of any ice on the shelves. Thus the ice volume $V_{\rm i}$ in (2) refers to all ice out to the grounding line and the surface area $A_{\rm o}$ is defined by this line and by the coastline.

The glacio-isostatic term $\Delta\zeta_{\rm I\text{-}g}$ in Eq. (1b) is the response of the sea surface to the changing ice load and the hydro-isostatic term $\Delta\zeta_{\rm I\text{-}h}$ is the response to the

concomitant change in water load. The two terms include contributions from the deformation of the crust under the surface load and from the change in the gravitational potential of the earth–ice–water system. Because the redistribution of melt water is a function of the deformation of the ocean basins and of the change in gravitational attraction by the ice, the two isostatic terms are coupled with $\Delta\zeta_{\text{I-h}}$ a function of $\Delta\zeta_{\text{esl}}$, $\Delta\zeta_{\text{I-g}}$ and $\Delta\zeta_{\text{I-h}}$ itself. Thus, the explicit separation of the two isostatic terms in (1b) is artificial and is done here only for illustrative purposes.

A key assumption made in formulating the isostatic terms is that the response of the earth to a surface load, of gravitational potential U, is linear. Thus, if the load is decomposed into potential harmonic constituents U_n, then for each harmonic both the deformation and change in gravitational potential are proportional to the corresponding harmonic U_n, with the proportionality coefficients defined by time-dependent load Love numbers. The evaluation of the response therefore reduces to the evaluation of the potential integrals of the ice and water loads on the deformable earth, with the requirement that ocean-ice mass is conserved and that the ocean surface remains an equipotential surface at all times. These assumptions have formed the base of most models for global isostatic rebound and associated sea-level change (e.g. Cathles, 1975; Peltier and Andrews, 1976; Nakada and Lambeck, 1987; Tromp and Mitrovica, 1999a, b), and the principal complexity is the evaluation of the Love numbers for realistic earth models and ensuring that the above-mentioned coupling is properly treated. Finally, rotational effects (Milne and Mitrovica, 1998) are included in the full formulation of Eq. (1).

The start time of the glacial loading history is taken either as the Last Interglacial (LIg) or an earlier interglacial, depending on whether the predictions are limited to the period since maximum glaciation or whether they include the full last cycle. The ocean boundary $O(t_{\text{o}})$ and depth $D(t_{\text{o}})$ at this start time is initially defined by the present geometry and the basin and coastline geometry is computed through time for a specified ice history and earth rheology up to the present time t_{P}. Because of earth-memory effects, this geometry $O(t_{\text{P}})$, $D(t_{\text{P}})$ may not be the same as the actual present-day values and the geometry through time is adjusted by subtracting out the difference between the starting geometry at LIg and the final geometry predicted for t_{P}. At each epoch, the ice thickness on the shelves is compared with the predicted depth of water to establish if the ice is grounded. If it is, the volume in (2) includes all ice grounded on the shelf. If it is not, the floating ice forms part of the water column along with the water layer between the base of the ice and the sea floor. When the shelf ice has thinned sufficiently for it to float, the ocean boundary is defined by the new location of the grounding line (Lambeck et al., 2003). Thus, the ocean geometry and the water depth must be known at each epoch and this is achieved through introducing high-resolution topography (including bathymetry) models into the solution of (1) and (2) and estimating the palaeo-topography/bathymetry

$$D(t) = D(t_{\text{P}}) - \Delta\zeta_{\text{rsl}} \tag{3}$$

as part of the iterative process. As the ice heights locally change linearly between integration time steps (see below), so does the ocean boundary evolve linearly between successive time steps.

In the first approximation, the glacio-isostatic term is evaluated from the integrals of the ice load defined for each epoch. In subsequent iterations, because the depth of the water column near the ice margins is a function of the gravitational attraction of the ice, and therefore of the ice itself, the evaluation of $\Delta\zeta_{\text{I-g}}$, is not independent of the water load and this interaction is included in the subsequent iterations. For illustrative purposes only, this is ignored in the next section and the first-iteration solution for $\Delta\zeta_{\text{I-g}}$ is used to provide an approximate estimate of the effects of the ice load on sea level in the Mediterranean. The first-iteration water-load correction assumes that the melt water is distributed uniformly over the oceans whose time dependence of area is defined by the boundaries $D(t_{\text{P}}) - \Delta\zeta_{\text{esl}} = 0$. In subsequent iterations, the water load is distributed according to the predicted sea-level change of the previous iteration and this allows the full coupling between the various components to be considered. Five iterations are found to be sufficient for present purposes but for some high-resolution analyses higher iterations are appropriate (e.g. Lambeck et al., 2004b). Here, again for illustrative purposes only, the water-load contribution is evaluated from

$$\Delta\zeta_{\text{I-h}} \approx \Delta\zeta_{\text{rsl}} - (\Delta\zeta_{\text{I-g}} + \Delta\zeta_{\text{esl}}), \tag{4}$$

where $\Delta\zeta_{\text{rsl}}$ is the fully coupled, multi-iteration solution and $\Delta\zeta_{\text{I-g}}$ is the first approximation glacio-isostatic term.

The a priori information required for predicting the glacially-driven sea-level change includes the definition of the earth's rheology, and a knowledge of the ice sheets through time. In reality, neither is necessarily known with adequate accuracy from ab initio considerations and both are evaluated in part from the analysis of glacial rebound responses. By analyzing sea-level responses from different geographic localities and at different times, and by combining the results with those from different responses (e.g. surface displacement measurements and moments of inertia and gravity change) some effective separation of ice- and earth-model parameters can be achieved. In particular, specific combinations of assumed ice sheet histories and rheological models can provide successful predictive

models for the isostatic response functions and for sea-level change.

2.2. Ice-volume equivalent sea-level (esl) function

Far from the former ice sheets, sea levels are subject to isostatic corrections $\Delta\zeta_{\rm I}$ that are typically 10–15% of the amplitude of the eustatic change. They are dependent largely on the total ice volumes, as expressed by $\Delta\zeta_{\rm esl}(t)$, and on the hydro-isostatic contribution $\Delta\zeta_{\rm I\text{-}h}(\varphi,t)$. Observations during the glacial cycle can therefore be corrected with some certainty to establish an estimate of the esl function as

$$\Delta\zeta_{\rm esl}(t) = \Delta\zeta_{\rm o}(\varphi,t) - \{\Delta\zeta_{\rm I}(\varphi,t) + \Delta\zeta_{\rm T}(\varphi,t)\}, \quad (5)$$

where $\Delta\zeta_{\rm o}(\varphi,t)$ is the observed value at (φ,t). Either data from tectonically stable regions are used (e.g. the Sunda Shelf (Hanebuth et al., 2000) or the Bonaparte Gulf (Yokoyama et al., 2000)), in which case $\Delta\zeta_{\rm T}(\varphi,t)=0$, or the elevations of known interglacial shorelines are used to correct for any tectonic effect (e.g. Barbados (Bard et al., 1990) or Huon Peninsula (Chappell and Shackleton, 1986)). For the present purpose, the esl function of Lambeck and Chappell (2001) is used for the interval from MIS 5.5 to MIS 2, and of Lambeck et al. (2002) for the Last Glacial Maximum (LGM) and post-LGM period. Two different representations for the Late Holocene will be used: (i) the nominal model in which all melting has ceased by 6.8 ka BP, and (ii) a model in which some Antarctic melting has continued until more recent time.

2.3. Ice sheet models

The global esl functions provide the boundary conditions for the total ice that can be contained within the sum of the individual ice sheets. The procedure we adopt for distributing this volume between the ice sheets is an iterative one in which glaciologically-derived ice models are used as a starting point, scaled such that their total volume is equal to the global esl function. In a second step, sea-level data from sites far from the ice sheets—far-field sites—are used to estimate global mantle rheology parameters. In the third step, rebound data from former glaciated regions are used to establish improved ice sheets, subject to the global mass constraint, as well as improved rheological parameters. In a fourth step, the far-field isostatic corrections are re-evaluated using the new ice models and a new esl function is estimated. The previous steps are then repeated until convergence is reached.

This process has been followed over several iterations with new ice sheets developed successively for the British Isles (Lambeck, 1993), Barents-Kara Sea (Lambeck, 1995a), Fennoscandinavia and Eurasia (Lambeck et al., 1998; Lambeck and Purcell, 2003), Greenland (Fleming and Lambeck, 2004), and North America (unpublished). Mountain glacier models have been adopted using known ice margins and volume changes given by Denton and Hughes (1981) with melting assumed to be in phase with the global deglaciation. The difference between the esl function for the northern hemisphere and mountain glaciations and the 'observed' function is used to define the history of the change in Antarctic ice volume $\Delta V_{\rm ant}(t)$. The distribution of ice across the continent, the ice margin retreat and ice-thickness change, is based on an interpolation between a scaled Denton and Hughes (1981) LGM reconstruction and the present ice sheet such that the total Antarctic ice mass is consistent with $\Delta V_{\rm ant}(t)$. If the testing of this model against rebound data for the Antarctic margin leads to a need to modify the ice sheet, then the sequence of analyses will be repeated in a next iteration.

The ice sheet models for the pre-LGM period are much more primitive than for the more recent time, and the current models used here assume that if at any pre-LGM time t' the esl value is equal to that for a post-LGM epoch t'' then $\Delta V_{\rm i}(t') = \Delta V_{\rm i}(t'')$. Tests with alternative hypotheses about the pre-LGM ice sheet indicate that this simple assumption is adequate only if the predictions are restricted to the LGM and post-LGM period.

In the case of the Mediterranean, the dominant ice sheets contributing to the isostatic components of sea-level change are the European ice sheet (Scandinavia, Barents-Kara, and Eurasia) and the western hemisphere ice sheets (Laurentide, Cordilleran, Arctic Canada, and Greenland). The Antarctic glacio-isostatic contribution is small and varies slowly across the region and the main contribution from this continent's ice volume change is through the water loading. Thus details of the Antarctic ice distribution are not important in this context and the preliminary model is adequate.

Complete ice models take into consideration the realistic time and spatial dependence of the ice loads on the continents and includes grounded ice on the shelves. Each of the northern ice sheets is defined at discrete time intervals, typically at 1000-year intervals, as prisms of 0.25° latitude by 0.5° longitude ($\sim 25 \times 25$ km) horizontal dimensions (this avoids the overlaps and creation of voids that occurs with disc representations). The Antarctic ice sheet is similarly defined but on a coarser $1^\circ \times 1^\circ$ grid. Melting of every prism at any location is assumed to be linear within each interval (Nakada and Lambeck, 1987).

2.4. Earth models

The time dependence of the earth's response appears to be well represented by simple models in which the

mantle viscosity distribution with depth is approximated by a small number of layers. The elastic parameters, including compressibility and density, vary with depth according to seismic data. Phase boundaries are assumed not to respond on the time scales of the glacial cycles and comparisons of model predictions based on this assumption with results in which the phase boundaries adjust instantaneously to the change in pressure do not indicate that this distinction is important in terms of producing parameters that describe the rebound (Johnston et al., 1997). For the models considered here a three-layered mantle is adopted comprising an elastic lithosphere of effective thickness H_1, an upper mantle of average effective viscosity η_{um} extending from the base of the lithosphere to the 670 km seismic discontinuity, and a lower mantle of effective viscosity η_{lm} extending to the core-mantle boundary. Tests for mantle models with a greater degree of layering show that such simple models capture most of the rebound signal.

Lateral variability in mantle viscosity, as well as in lithospheric thickness is ignored. This is on the grounds that there is no observational database that would be satisfactory for inversion for both the ice-model parameters and the depth-lateral distribution of viscosity. However, regional inversions of sea-level data do indicate that there may be some lateral variability in effective upper-mantle viscosity in a range of $\sim 10^{20}$ Pa s for the South Pacific mantle to $\sim 5\text{–}6 \times 10^{20}$ Pa s for the mantle beneath North America. This provides one of the rationales for carrying out regional solutions, rather than a single global solution, on the basis that much of the regional deformation recorded is more indicative of the mantle rheology beneath the loaded area than of the mantle beyond this region. A number of solutions indicate that representative values for the upper-mantle viscosity beneath continental margins and away from the cratonic cores of Scandinavia and North America, and including the Mediterranean, are in the range $(2\text{–}4) \times 10^{20}$ Pa s (e.g. Lambeck and Nakada, 1990; Lambeck and Bard, 2000; Lambeck et al., 2004a). The lower-mantle viscosity is reasonably well constrained by sea-level data from far-field sites because the wavelength of the water loads, defined by the ocean basins, is equal or greater than the depth of the mantle. Also, the time dependence of the inertia tensor of the planet, as recorded in the orbital perturbation spectrum of close earth satellites or in the planetary rotation, provide good constraints on lower-mantle viscosity (e.g. Kaufmann and Lambeck, 2002) and we adopt values of $(5\text{–}20) \times 10^{21}$ Pa s. Effective values for the elastic thickness of 50–80 km also appear to be appropriate. Independent solutions for mantle rheology give similar results (e.g. Mitrovica, 1996; Mitrovica and Forte, 1997; Milne et al., 2001).

3. Model predictions across the Mediterranean basin

3.1. Sea level on a rigid earth

Without deformation of the solid earth, the sea-level function is determined by the gravity of the surface load of ice and redistributed meltwater such that the sea-surface remains at constant gravitational potential. Fig. 1a illustrates this contribution at 12 ka BP (it is zero at 6.8 ka as in this model there is no further change in the ice history from this time to the present) for the iterative solution of Eq. (1) in which the mantle viscosity has been set to an infinitely large value. The pattern is a quasi-uniform gradient across the region with levels above the esl value of ~ -54 m for this epoch. This is the result of the broad zone that develops around each of the northern hemisphere ice sheets in which the sea surface is deflected upwards by the gravitational attraction of the ice. The North American influence is seen mainly as a NW–SE slope of about 3.5 m from the Golfe du Lion (France) to Egypt whereas the Scandinavian signal is a predominantly N–S gradient of about 0.5 m from Trieste to the Gulf of Sirte (Libya) and together they form the broad pattern shown in Fig. 1a. (By 12 ka BP the percentage reduction in ice volume of Scandinavia has been greater than for North America, and despite the greater distance to it, the North American ice load dominates the signal. At the time of the LGM, the gradients are more comparable, ~9 m for the NW–SE slope towards North America and ~7.5 m for the N–S slope towards Scandinavia.) The small 'wiggles' in the contours in Fig. 1a at the land–water boundaries, such as across Italy or the Aegean Sea or the larger ones across the coast of North Africa, are the result of the changing gravitational attraction between water and land as sea level rises. The Antarctic influence is predominantly the constant equivalent sea level for the epoch.

3.2. Glacio-isostatic contributions

Figs. 1b and c illustrate the glacio-isostatic contributions to relative sea level at 12 ka BP from the individual ice sheets over northern Europe and North America, respectively, and the signal is primarily due to the change in deformation of the planet between 12 ka and the present rather than to the change in direct gravitational potential of the ice sheet. The result is a concentric pattern of subsidence of the broad uplift zone created during the time of ice growth around each of the ice sheets. Also illustrated (Fig. 1d) is the contribution from the Alpine deglaciation for the same epoch and within the marine environment, this contribution is significant only in the northern Adriatic and Gulf of Genoa areas, reaching 4–5 m at 12 ka BP and 1–1.2 m at 6 ka BP.

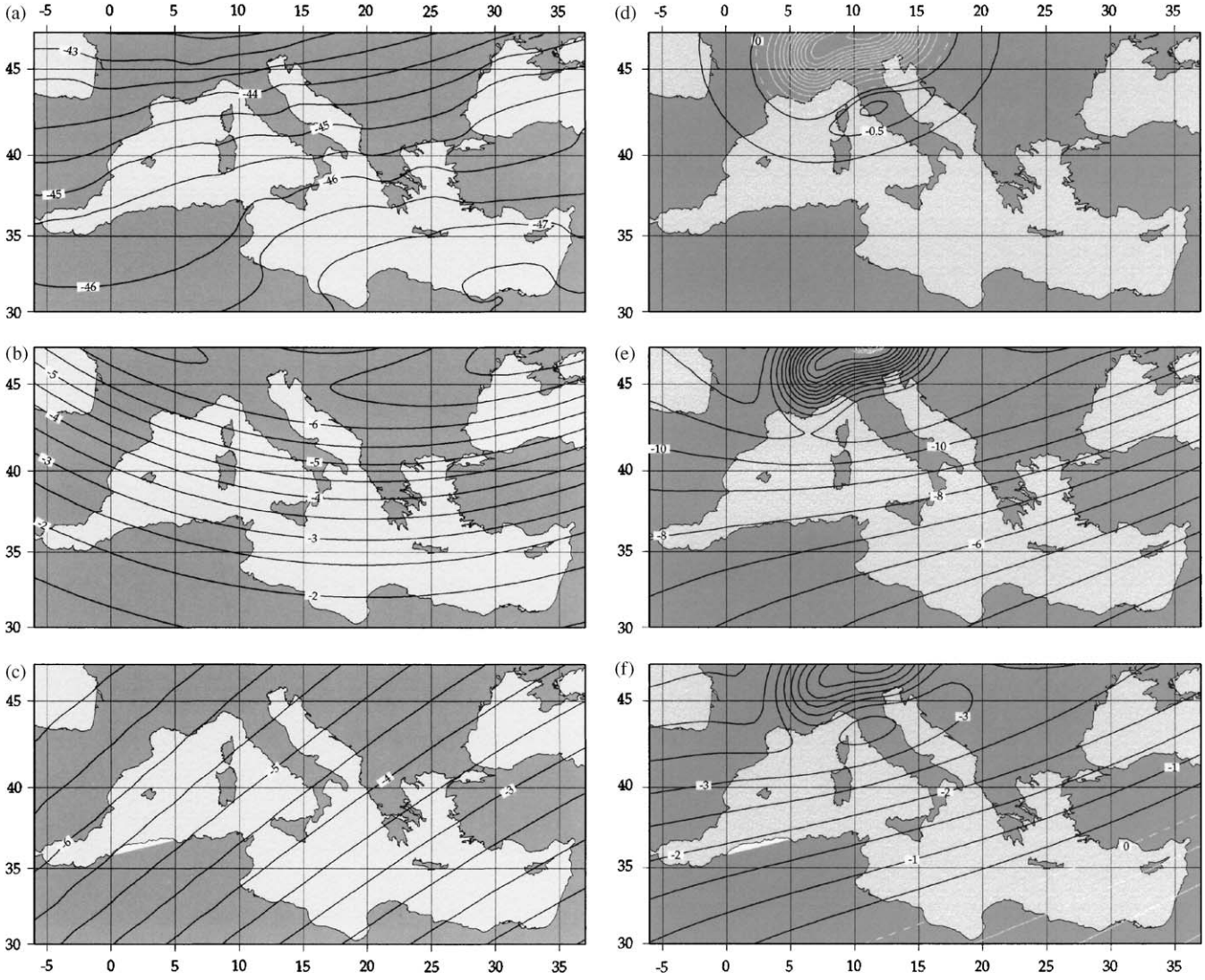

Fig. 1. (a) Relative sea-level change between 12 ka and present for the melting of the nominal ice sheets on a rigid earth. The equivalent sea level at 12 ka BP is −54 m and across the region water levels lie above this level because of the direct gravitational attraction of the water by the northern ice sheets. (b) The glacio-isostatic contribution $\Delta\zeta_{I-g}$ at 12 ka from the decay of the northern European ice for the nominal earth model. (c) Same as (b) but for the North American ice sheet. (d) Same as (b) but for the Alpine deglaciation. (e) The glacio-isostatic contribution at 12 ka BP from the total global ice sheets, including Antarctica and mountain glaciers, (f) Same as (e) but for 6 ka BP. In all model predictions, melting ceased at 6.8 ka BP. The black contours denote negative values, white contours positive values, and the zero contour is given by the dashed white line. In (d) the contour interval is 1.25 m and the maximum value is ~11 m. (At 6 ka BP, the maximum value for the central Alpine rebound is ~3 m.) A small peripheral bulge develops around this alpine load with maximum deflection in central Italy of about 1 m at 12 ka (and 0.25 m at 6 ka BP).

The total $\Delta\zeta_{I\text{-}g}$ for all ice sheets, including an Antarctic contribution, is illustrated in Figs. 1e and f for 12 and 6 ka, respectively. For the former epoch, the change across the region from the glacial rebound alone ranges from about −3 m in the eastern Mediterranean to about −12 m for the northern Adriatic Sea and the French Mediterranean coast. Under the influence of the Alpine rebound, the gradient changes sign in both the northern Adriatic Sea and the Gulf of Genoa, and the largest magnitudes for $\Delta\zeta_{I\text{-}g}$ actually occurs in the central northern Adriatic. The pattern illustrated in Figs. 1e and f persists for much of the Holocene except that by 6 ka small positive values for $\Delta\zeta_{I\text{-}g}$ are predicted for the far-eastern Mediterranean where the long wavelength direct attraction is of larger amplitude than the deformational contribution. Other than here, the glacio-isostatic effect across the region is mostly one of a rising level in Late Holocene time, even when ocean volumes have remained constant since 6.8 ka BP.

3.3. Hydro-isostatic contribution

Figs. 2a and b illustrate the hydro-isostatic contribution $\Delta\zeta_{I\text{-}h}$ across the region at 12 ka BP. Two results are

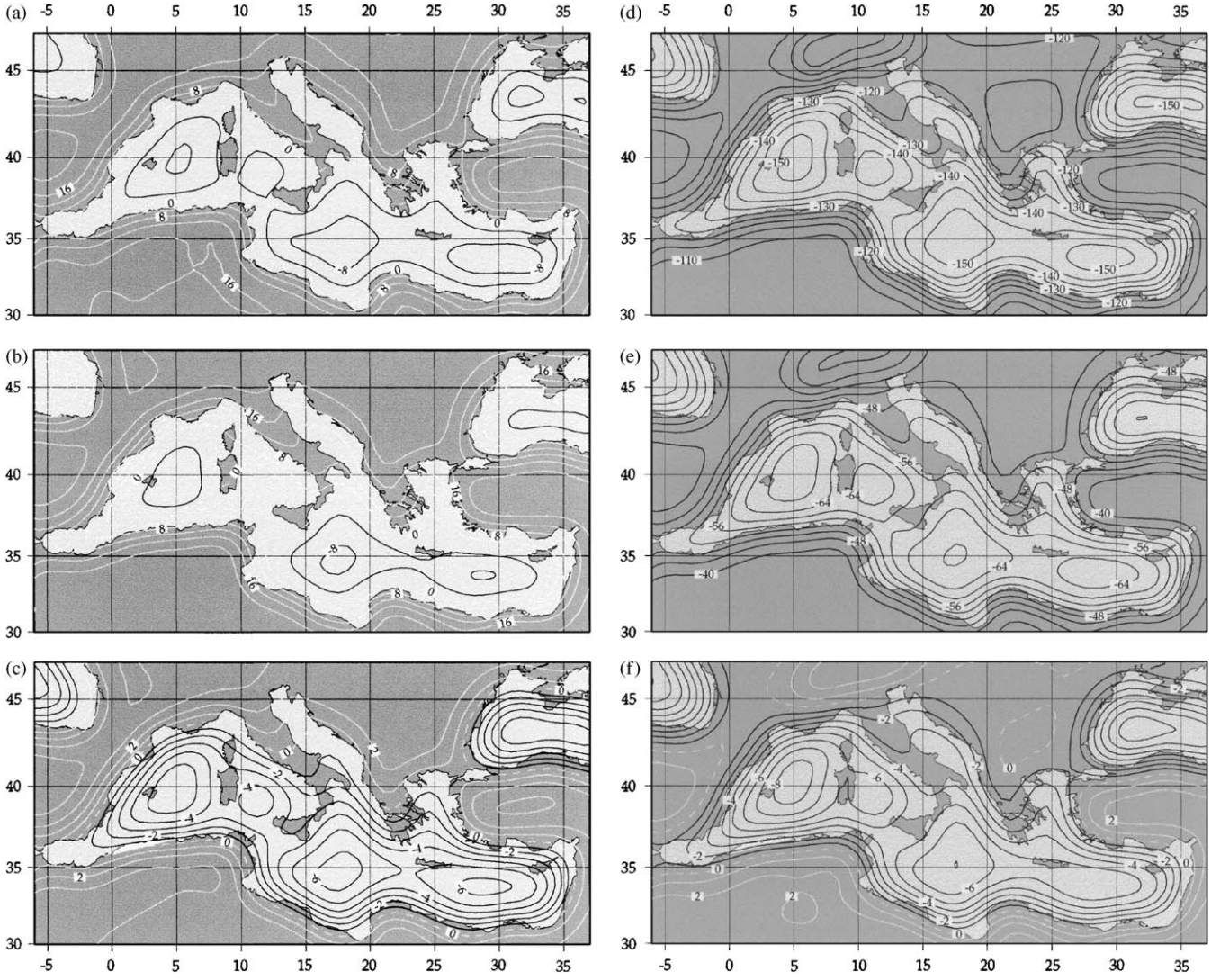

Fig. 2. (a,b) Hydro-isostatic contributions $\Delta\zeta_{I-h}$ at 12 ka BP corresponding to the decay of the global ice sheets with cessation of melting at 6.8 ka BP. (a) The first-iteration solution of the sea-level equation in which the water load is represented by a globally uniform water load equal to the equivalent sea-level for the epoch. (b) The fifth-iteration solution of the sea-level equation in which the coupling between the various terms is fully incorporated and the water-load definition is gravitationally consistent with the potential of the earth–ocean–ice system and with the shoreline and ice-grounding lines for the epoch. (c) Same as (b) but at 6 ka BP. (d–f) The total predicted relative sea-level change at 20, 12 and 6 ka BP, respectively, for the nominal earth and ice model, including $\Delta\zeta_{I-g}$ and $\Delta\zeta_{I-h}$. The contour notation is the same as in Fig. 1.

shown: the first is for the first-iteration solution of the sea-level equation in which the water load added into the global oceans is represented by a slab of uniform thickness equal to the change in esl. In the local isostatic limit, the sea-floor subsidence would be $(\rho_{ice}/\rho_{mantle})\,\Delta\zeta_{esl}$ or ~15 m at 12 ka BP. In the same limit, the displaced mantle material uplifts the non-loaded continents by a maximum of about twice this amount (ocean/land area $\approx$ 2) and the relative sea-level change at the crustally-sheared coast lines (of a local isostatic model) would be ~45 m. The local isostatic state would not be reached at the ocean–land boundaries unless the lithosphere failed and the maximum relative sea-level change here will, by analogy of loading of an infinite elastic layer over a fluid by a semi-infinite slab load, be approximately 50%, or about 20–25 m, across the coastal zone. From Fig. 1e, the water load for the Mediterranean basin is greater than the esl value for this epoch by between ~10% and ~20% and the actual water-load magnitude will exceed that for this simple esl slab model. Thus the fully coupled models will be required (Figs. 2b and c) and these modify the first iteration result in two important ways: (i) some of the water-load displaced mantle material will compensate for the rebound beneath the ice-loaded areas, and (ii) the thickness of the water column is modified by the glacio-

isostatic adjustment and by the gravitational change. The pattern of change remains the same as for the first-iteration solution but the amplitudes are modified.

3.4. Relative sea-level change

The relative sea-level change, including the gravitational and deformational parts of both isostatic terms and the esl contributions, is illustrated in Figs. 2d–f for the epochs 20, 12 and 6 ka BP, always for the nominal earth and ice models, with equivalent levels at these epochs of −142, −54 and 0 m, respectively. The local levels at the time of maximum glaciation vary from −110 to −150 m across the region and are below the esl values near the centers of the sub-basins south of Italy, between Majorca and Sardinia, and in the eastern Mediterranean. The shallower values occur within the Gulfs of Genoa and Lion and in the northern Adriatic. (See Fig. 3 for locations.) At 12 ka BP, the levels range from ~−40 m in the northern Adriatic to <−68 m near the centers of the above-mentioned basins. The pattern is similar to that at 20 ka BP, with the levels at the coast being mostly above the esl values whereas offshore they are mostly below the esl values. At both epochs, the pattern follows closely the coastline geometry, indicative of water loading contributing a major role to the spatial variability of the overall isostatic signal (c.f. Fig. 2a). This pattern persists for other Late Glacial and Holocene periods. At 6 ka BP, for example, sea levels remain below present day across much of the region, the two isostatic contributions being both negative. The exceptions occur in the northernmost Adriatic and along segments where the North African coast is indented, such as in the Gulfs of Sirte and Gabé, and along the easternmost Mediterranean coast (Fig. 2f). In the northern Adriatic, the small positive values at this

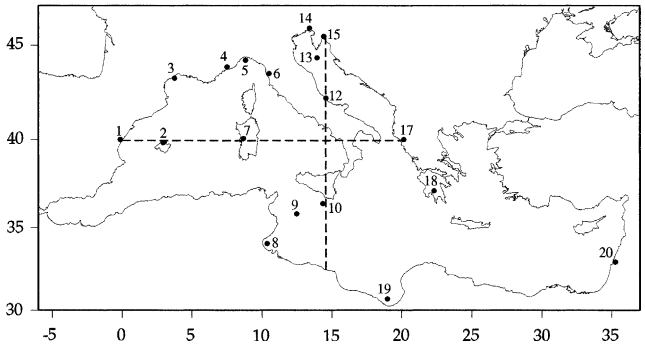

Fig. 3. Location map of principal sites mentioned in text. 1: Castellan, Spain. 2: Majorca and Balearic Islands. 3: Golfe du Lion. 4: Côte d'Azur. 5: Golfo di Genova. 6: Versilia Plain, Italy. 7: Sardinia. 8: Golfe de Gabés. 9: Lampedusa. 10: Malta. 11: Golfo do Salerno. 12: Ortona. 13: North Adriatic. 14: Trieste. 15: Susak, Croatia. 16: Golfo di Taranto. 17: Albania. 18: Peloponnisos. 19: Golfe de Sirté. 20: Carmel Coast, Israel. The dashed lines correspond to the sections in Figs. 4 and 6.

epoch are a consequence of the inclusion of the Alpine glaciation and precise observations of the sea-level gradient along the coast may be useful for placing approximate limits on the magnitude of the Alpine ice load. Along parts of the North African and Levantine coast, the two isostatic contributions are of opposite sign with the water load being dominant, resulting in predictions of small-amplitude highstands in Late Holocene time. Notably, the predicted levels along the Gulfs of Sirte and Gabès coasts exhibit strong spatial gradients, for example, ~4 m from Gabès to Tunisia, and data from this region would be important for evaluating model parameters appropriate for the region. Between Majorca and Sardinia, the predicted levels for 6 ka BP lie as much as 8 m below present, and the spatial variability remains significant across the entire region and considerably greater than most observational uncertainties.

4. Precision of sea-level predictions

4.1. Dependence on earth-model parameters

The above predictions are based on the nominal earth model for a three-layered mantle. No systematic inversion of sea-level data for the entire Mediterranean has yet been attempted, but a number of regional solutions—from France, Italy, Greece, and Israel—all indicate that parameters in the range given in Table 1 yield predictions that are consistent with observations (Lambeck, 1995b; Lambeck and Bard, 2000; Sivan et al., 2001; Lambeck et al., 2004a). The earth-model dependence of the predictions for this parameter range is illustrated for two epochs (6 and 12 ka BP) in Fig. 4, along two profiles, a north–south profile from the northern Adriatic to North Africa and an east–west profile along 40°N in the western Mediterranean. For $t = 6$ ka BP, some of the largest differences occur near the centers of the sub-basins within the Mediterranean (e.g. Menorca, or between Sicily and North Africa) but they are smaller at the coasts of the larger land bodies (e.g. North Africa or Castellan) and mostly no larger than the observational uncertainties for Late Holocene epochs. The pattern is similar for $t = 12$ ka. Thus, within the Mediterranean basin there are locations where the predictions are relatively insensitive to earth-model parameter choice and data from these would constrain primarily the esl function. Then there are other localities where the earth-model dependence is substantial and by an appropriate selection of sites and epochs it should be possible to invert sea-level data from the region to improve upon the rheological parameters, particularly if basin-wide data are available for the entire post-LGM interval. Until such an analysis is completed, we adopt the nominal earth-model parameters defined in Table 1

Table 1
Summary of parameters for the three-layered mantle model

Earth model	Lithospheric thickness (km)	Upper mantle viscosity ($\times 10^{20}$ Pa s)	Lower mantle viscosity ($\times 10^{22}$ Pa s)
El	65	2	1
E2 (nominal)	65	3	1
E3	65	4	1
E4	50	3	1
E5	80	3	1
E6	65	3	0.5
E7	65	3	2

E2 is the nominal model and the other models represent the range of parameters that are consistent with rebound analyses in the Mediterranean region and elsewhere.

and as estimates of precision we use the root-mean-square of the predicted variability, relative to the nominal solution, for the models defined in Table 1. Figs. 4e and f illustrate these precision estimates for the two transects at 6, 12, and 20 ka.

4.2. Ice-model dependence

Uncertainties in the ice sheet models enter into the sea-level predictions through both the esl function and through the isostatic terms. The latter follows from comparisons of predictions for different representations of the ice sheets. For northern Europe, including the Barents-Kara region, two ice models are used. The first, NE-1, from Lambeck et al. (2000), is characterized by a thick LGM ice sheet that experienced a rapid reduction in thickness at 19 ka BP. The second, NE-2, is the nominal northern European model used above. It is the result of more recent iterative inversions in which additional field data have been used, including constraints on ice thickness during the late stages of deglaciation of Sweden as well as information from the drainage history of the Baltic (Lambeck and Purcell, 2003). The principal difference between the two is that in NE-2 there is less ice during both the LGM and the late stages of deglaciation compared with NE-1 (Fig. 5).

Two different ice models have been used for the North American ice sheet. NA-1, is based on the original ICE-1 model of Peltier and Andrews (1976) but scaled in amplitude so that when combined with the other ice sheets, the resulting esl function is consistent with the observed values (Lambeck et al., 2002). NA-2, the nominal model used above, is based on inversions of observed data compiled by Tushingham and Peltier (1992) and two glaciologically-based starting models of Peltier and Andrews (1976) and Licciardi et al. (1998). Model features common to the different inversion solutions, that are independent of the starting ice-sheet models and are consistent with observational data, define the model NA-2. Compared with NA-1, this model is characterized by a multi-domed ice sheet, a larger ice volume at the time of the LGM, advanced melting for the early deglaciation stage, and delayed melting during the late stage of deglaciation.

Fig. 6 illustrates the comparisons of the glacio-isostatic terms at 6 and 12 ka BP, along the same profiles as before. The amplitude of the isostatic signal in the Mediterranean basin due to the northern European ice sheet, for example, is ~6% of the total change at the LGM and ~10% at 12 ka BP and uncertainties in the ice volumes of the order of 10–20% should not introduce major uncertainties into the glacio-isostatic predictions. This is indeed the case, with the maximum differences resulting from either the two European models or the two North American models not exceeding 1 m at 6 ka BP and ~2 m at 12 ka BP. We therefore adopt the nominal models NE-2, NA-2 and use the differences in model predictions between NE-2 and NE-1 and NA-2 and NA-1 as a measure of uncertainty. This gives the results illustrated in Figs. 6e and f for the two profiles and at three epochs. In most cases, the uncertainty introduced from this source is less than observational uncertainties for the same epochs.

4.3. Equivalent sea-level dependence

The nominal esl function is based on Eq. (5), using data from a number of far-field localities around the world. For each observed data point, the accuracy of the inferred esl value is based on the observational accuracy and on the precision of the isostatic correction (Lambeck et al., 2002). The esl-reduced observations can then be combined into a time-dependent esl function whose precision is estimated from the scatter of results. The resulting error function (Lambeck et al., 2004a) is illustrated in Fig. 7a and the precision estimates range from ~0.4 m at 6 ka BP to ~5 m at the LGM.

4.4. Precision of sea-level predictions

The variances of the predicted sea levels are estimated as the sum of the variances of the three principal contributions: earth model, ice sheet, and esl function uncertainties. The resulting spatially variable estimates are illustrated in Figs. 7b and c for the two Mediterranean profiles at the epochs 6, 12 and 20 ka BP. The dominant contribution to these estimates comes from the esl function, a consequence of which is that the uncertainty of the relative sea-level predictions are primarily time dependent. Their magnitudes, ~1, 3.5, and 5.5 m at 6, 12, and 20 ka, respectively, are comparable to the uncertainties of much of the observational evidence for the region and the model predictions should provide a sound basis for modeling

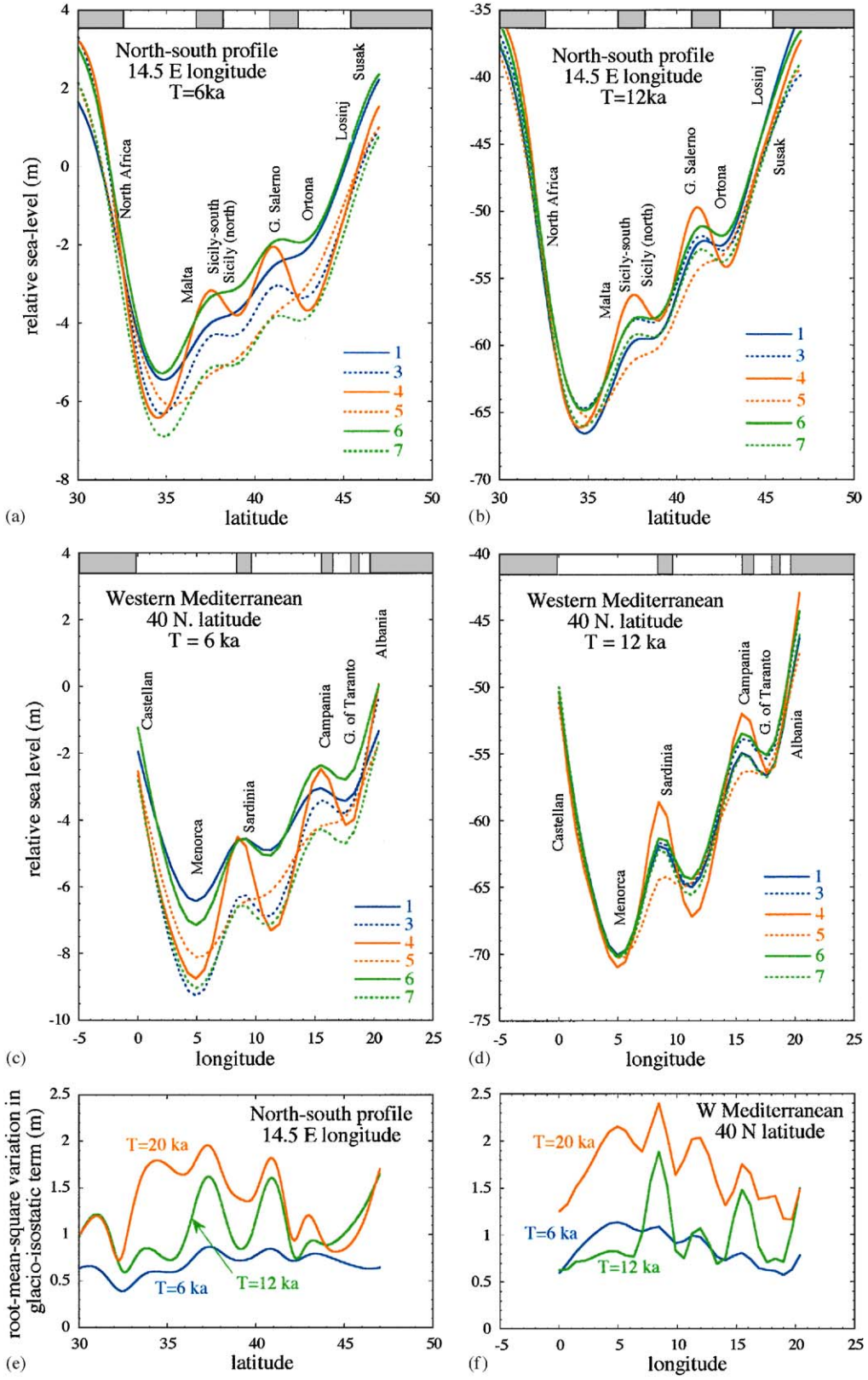

Fig. 4. Predicted sea levels at two epochs, 6 ka BP (a,c) and 12 ka BP (b,d), along (a,b) a north–south profile at ~14° east and (c,d) a west–east profile at ~40° latitude (see Fig. 3 for locations). The results are for the nominal global ice model with constant ocean volume for the last 6.8 ka and for the range of earth models summarized in Table 1. (e,f) Precision of the sea-level predictions for the nominal earth-model parameters due to the uncertainty of earth-model parameters.

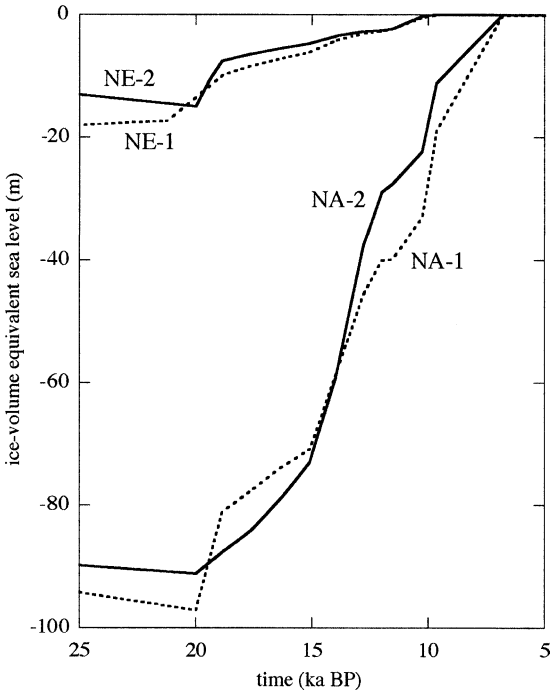

Fig. 5. Ice-volume equivalent sea-level function for the northern European (NE-1, NE-2) and North American (NA-1, NA-2) ice models. NE-2 and NA-2 are components of the global nominal ice model.

LGM and more recent sea-level change and shoreline migration across the region at this level of accuracy.

4.5. Separation of earth-model parameters

The brief analysis above of the earth-model dependence indicates that some separation of earth-model parameters is possible if the observational data is appropriately distributed in space and time. As an example, Fig. 8a illustrates the difference in predicted values at 6 ka BP for two models with different lithospheric thickness H_1 (E4–E5, Table 1) for the Mediterranean region. Within this range the dependence of the predicted levels on H_1 is approximately linear (Fig. 10, below) so that the zero contour represents locations where the relative sea-level predictions are least sensitive to the choice of lithospheric thickness. A similar result for 6 ka BP is illustrated in Fig. 8b for the dependence on upper-mantle viscosity $\eta_{\rm um}$ (E1–E3), and locations can be identified where this dependence is small and comparison of the H_1 and $\eta_{\rm um}$ results indicates that there is some orthogonality of these sensitivity contours. In western Sardinia, for example, the predictions are insensitive to H_1 but are more sensitive to $\eta_{\rm um}$. Elsewhere, the predictions are insensitive to either of these parameters within their respective ranges, but they are sensitive to the choice of lower mantle viscosity (c.f. Fig. 8c), such as along the coast of North Africa, and results such as these provide a guide to which observation sites and which epochs are most important for ensuring separability of mantle parameters.

5. The equivalent sea-level function during Late Holocene

Of the potential limitations of the sea-level prediction model, the most significant one probably concerns the choice of esl function, particularly for the Holocene period. With the assumed disappearance of the last of the Laurentian ice sheet at ~6.8 ka BP in the above ice models, ocean volumes have remained constant for the past 6800 years. But there are no a priori reasons why ongoing Antarctic melting or mountain glacier decay could not have resulted in ocean volumes increasing into Late Holocene time. For example, recent evidence from Mary Byrd Land, Antarctica, indicates that a significant lowering of the ice surface has occurred in Late Holocene time over a large area and that this may have contributed as much as 1 m to global level (Stone et al., 2003). Or, estimates of mountain glacier melting for the past century indicate a sea-level rise of ~0.2–0.4 mm/year (Meier, 1993; Oerlemans, 1999) which, *if* representative of the past 7000 years, would result in an esl rise of ~1.5–3 m. Thus, our analyses of sea-level data for rheology and ice parameters have generally included the esl function as an unknown (e.g. Nakada and Lambeck, 1987; Lambeck, 2002).

Across the Mediterranean, there are localities where, at different times, the predicted values are equal to the esl values and data from these localities are particularly valuable for estimating corrections to this latter function. For example, at 6 ka BP, the predicted levels along the Levant coast are nearly zero (Fig. 2f) and any observed levels from these localities should provide a quite direct measure of the esl value for that epoch. At 12 ka BP, the model esl value is −54 m and this contour in Fig. 2e identifies locations, such as along the northern Tyrrhenian coast of Italy or in the Golfe du Lion, where any observations should provide a direct measure of the esl value. Similarly, at 20 ka BP, the relative sea level equals the esl value at locations such as near Malta and Lampedusa or the Balearic Islands. These locations will vary with earth-model parameters and the challenge will be to identify locations where the isostatic terms are both small and insensitive to at least some of the mantle parameters.

Consider observed sea level $\Delta\zeta_{\rm o}$ at two locations φ_1, φ_2 for the same epoch t and far from former ice sheets such that the total isostatic corrections $\Delta\zeta_{\rm I}$ are small. Then

$$\Delta\zeta_{\rm o}(\varphi_1, t) = \Delta\zeta_{\rm esl}(t) + \Delta\zeta_{\rm I}(\varphi_1, t),$$
$$\Delta\zeta_{\rm o}(\varphi_2, t) = \Delta\zeta_{\rm esl}(t) + \Delta\zeta_{\rm I}(\varphi_2, t),$$

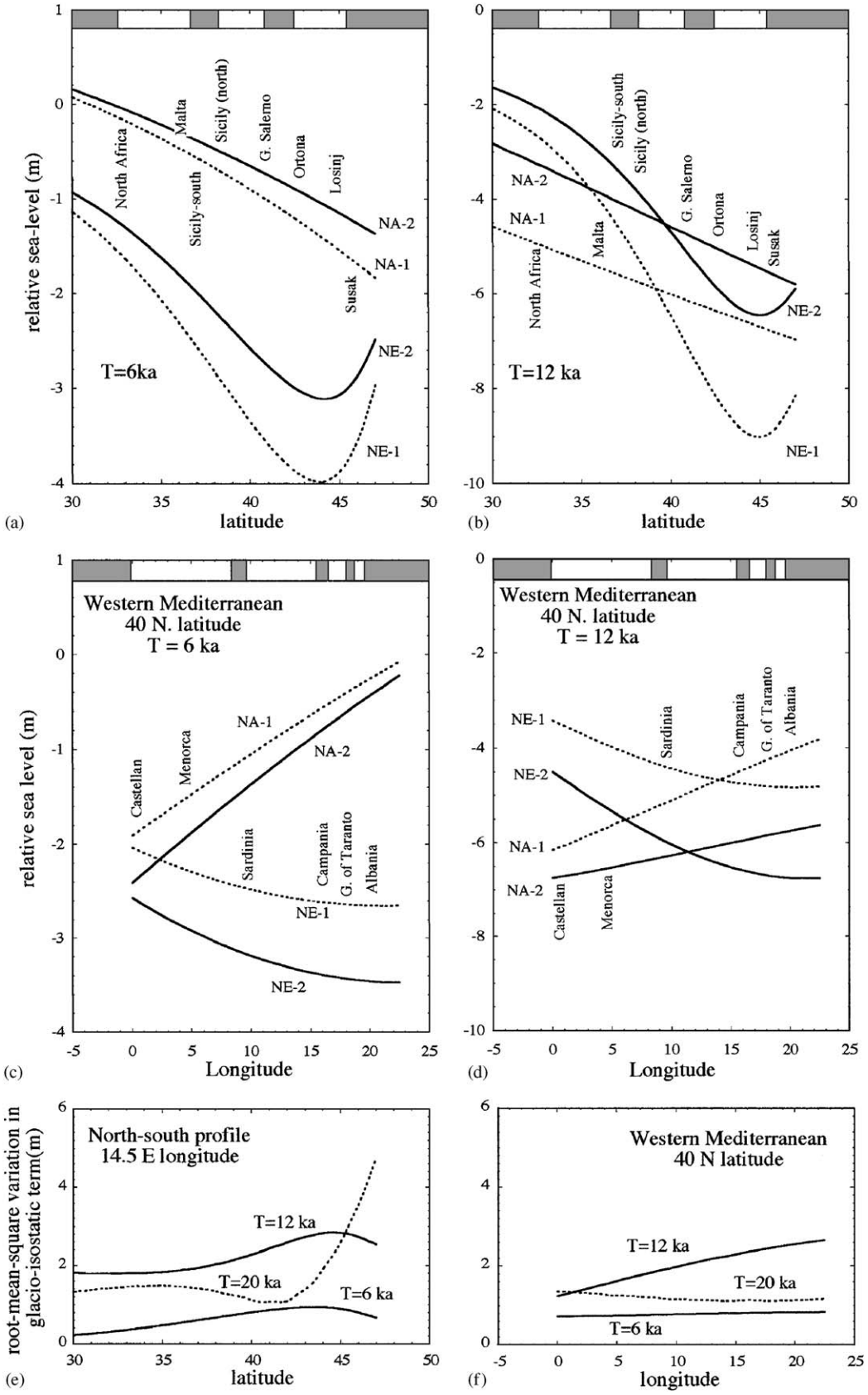

Fig. 6. (a–d) Predicted glacio-isostatic contributions to sea level at 6 ka BP (a,c) and 12 ka BP (b,d) along the same two profiles as in Fig. 4 for the northern European (NE-1, NE-2) and North American (NA-1, NA-2) ice loads. (e,f) Precision of the sea-level predictions based on the nominal ice model arising from uncertainty in the ice models at 6, 12, 20 ka BP.

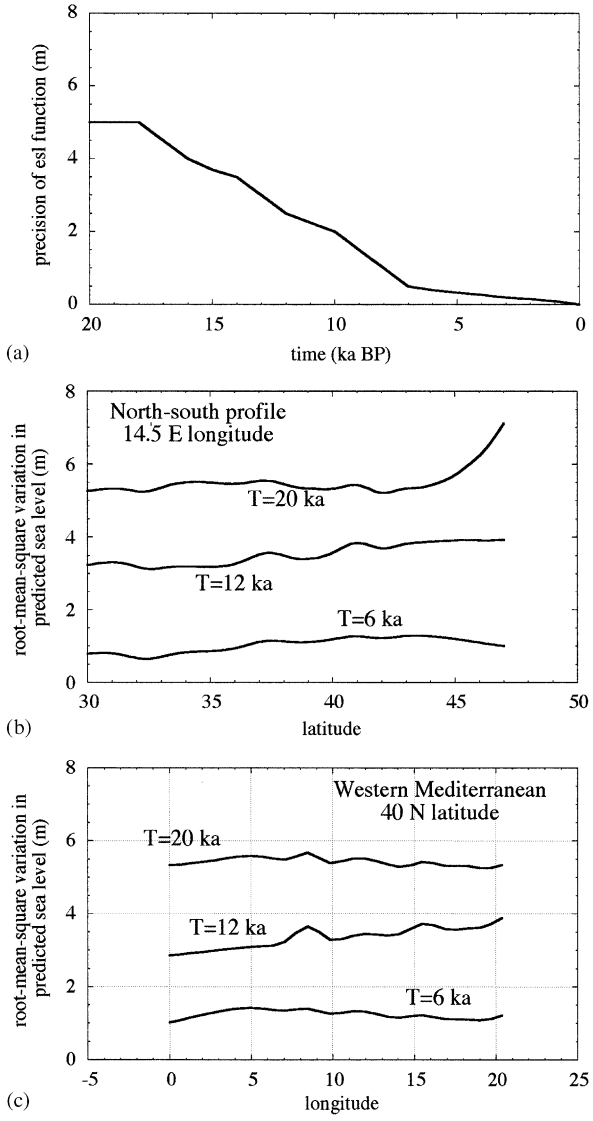

Fig. 7. (a) Precision estimates of the equivalent sea-level function. (b,c) Precision estimates for the sea-level predictions along the two profiles of Fig. 4 at 6, 12, and 20 ka BP. These estimates include uncertainties arising from the earth-model parameters (e.g. Figs. 4e and f), ice-model parameters (e.g. Figs. 6e and f), and the a priori esl function (a). The uncertainty of the Alpine glaciation model has been arbitrarily set to 30% of the ice thickness estimates for the individual ice caps.

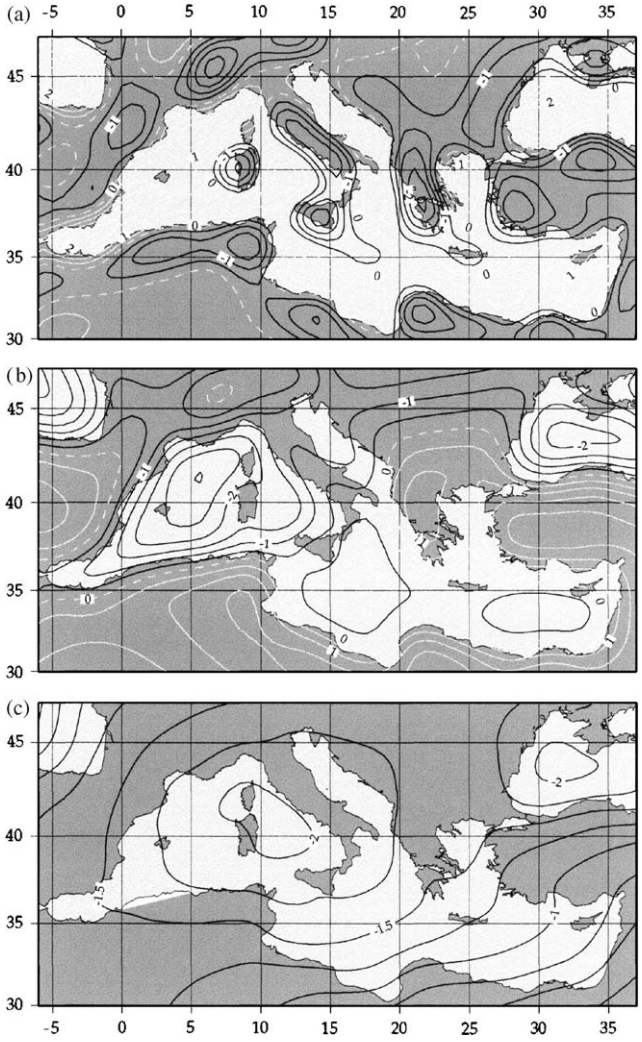

Fig. 8. Predicted differences in sea level for pairs of earth models (see Table 1 for notation). All results are for 6 ka BP. (a) E4–E5, representing two models that differ only in effective lithospheric thickness. (b) E1–E3, representing two models that differ only in effective upper-mantle viscosity. (c) E6–E7, representing two models that differ only in effective lower-mantle viscosity. The zero contour (white dashed line) indicates locations where the response is insensitive to the parameters within the range considered.

and the difference

$$\Delta\zeta_o(\varphi_1,t)-\Delta\zeta_o(\varphi_2,t)=\Delta\zeta_I(\varphi_1,t)-\Delta\zeta_I(\varphi_2,t) \quad (6)$$

is independent of $\Delta\zeta_{esl}$ in a first approximation. (Recall that $\Delta\zeta_I$ is a function of $\Delta\zeta_{esl}$ and an iterative procedure may be required.) This difference will be dependent primarily on mantle rheology and, if the isostatic variation is substantial across the region, can be inverted for the earth-model parameters (c.f. Fig. 8). Once these parameters are determined, the isostatic corrections are evaluated and the esl estimates follow.

This approach requires that the regional isostatic variability is substantial across the region analyzed so that the earth-model parameters can be separated. This condition can sometimes be met (c.f. Lambeck and Nakada, 1990) and several analyses have suggested that during the past 7000 years ocean volume has increased so as to raise the global level by 2.5–3 m, with much of this change having occurred in the interval from ~7 to ~3 ka BP (Lambeck, 2002). The pattern of spatial variability of the sea-level change across the Mediterranean and the estimates of precision for the model predictions suggests that data from this region also has the potential to test the hypothesis that ocean volumes have not remained constant for the past 7000 years. To illustrate this, we consider data from several locations

across the region. A more complete analysis using a much more substantial data set is in progress.

5.1. Carmel coast, Israel

Archaeological evidence from several sites indicates that sea levels between 6.3 and 6.9 ^{14}C ka BP occurred from 4.5 to 7 m below present and that levels remained below or close to present from ~6 ka BP to the present (Galili et al., 1988; Galili and Nir, 1993; Sivan et al., 2001), consistent with the recent analysis of the well data from Caesarea (Sivan et al., 2004). The area appears to be tectonically stable because the present-day position of shallow marine MIS 5.5 sediments is consistent with little vertical tectonic movement for the past 120 ka and with the gradient of the Roman aquaduct bringing water to Caesarea being preserved over 2000 years. The sea-level predictions for the range of earth models from Table 1 and for ice-sheet models in which all melting ceased at 6.8 ka BP are illustrated in Fig. 9a. The abrupt change in gradient at 6.8 ka BP is the consequence of the equally abrupt end of melting at this time and the

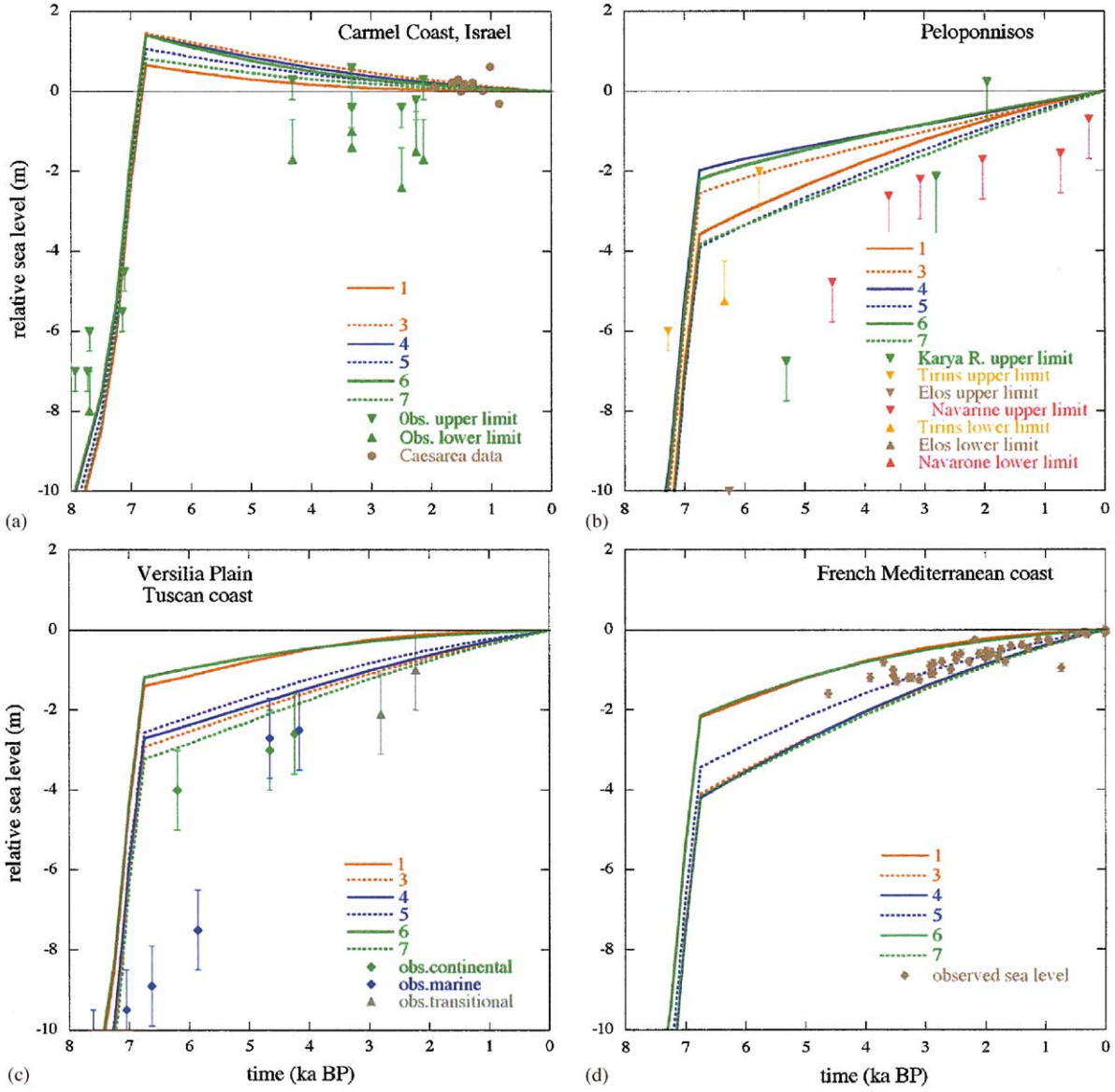

Fig. 9. Comparison of observed and predicted sea levels at four Mediterranean sites. The predictions are for the nominal global ice model with zero change in ocean volume after 6.8 ka BP, and for the range of earth-model parameters summarized in Table 1. (a) The Carmel coast of Israel, including Caesaria. Upper and lower estimates of sea level are indicated. Data is from various sources summarized by Sivan et al. (2001, 2004). (b) Peloponnisos, Greece. The data is from several sites (Gulfs of Argolid, Messini, Elos and from Navarine Bay) and the predictions are for Tirins. The field data is from Kraft and Rapp (1975) and Kraft et al. (1977, 1980) and has been summarized by Lambeck (1995b). (c) Versilia plain, Tyrrhenian coast of Italy. The field data is from Antonioli et al. (1999a). (d) Côte d'Azur, France. The data includes the vermetid and coralline algae information from Laborel et al. (1994) and archaeological information from Morhange et al. (1996).

change would become more gradual if the ocean volume continued to increase slowly. The absence of such an abrupt change in any observational record would, therefore, be indicative of ongoing ocean volume change at this time. Significant is that for the range of models the Late Holocene predictions are consistently above present and higher than the observed values (Fig. 9a) unless the mantle viscosities lie outside the range considered. An increase in lower-mantle viscosity to values above 2×10^{22} Pa s has the effect of lowering sea level, but the dependence becomes small for this location as is illustrated in Fig. 10b. Likewise, the lithospheric dependence is not large here (Fig. 10c) and higher values for the effective thickness have only a small effect on the amplitude highstand.

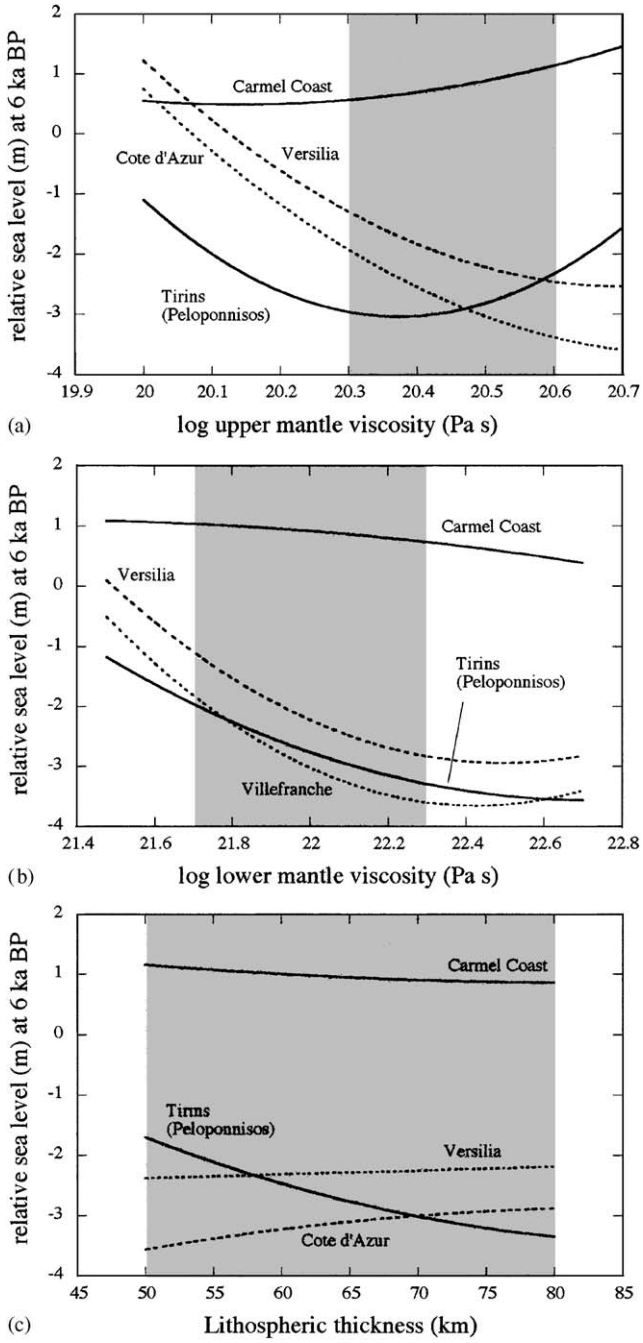

Fig. 10. Earth-model parameter dependence of relative sea-level predictions for 6 ka BP at four Mediterranean sites. The grey-tone areas define the parameter range of Table 1. (a) Dependence on upper-mantle viscosity, (b) dependence on lower-mantle viscosity, and (c) dependence on lithospheric thickness.

5.2. Peloponnisos, Greece

Evidence for Holocene sea-level change is available from several localities at the heads of the Gulfs of Argolid, Messini and Elos and at Navarine Bay (Kraft and Rapp, 1975; Kraft et al., 1977, 1980) where tectonic stability is suggested by the occurrence of the Last Interglacial sea levels at a few meters above their present level (Kelletat et al., 1976; van Andel, 1987). Some small spatial variability between these sites is predicted (~0.5 m at 6 ka) (Lambeck, 1995b) but the information here has been combined into a single curve for illustrative purposes only. The evidence includes very shallow marine sediments, providing lower limits, but most of the evidence for the past ~7 ka is from shallow-lagoonal and back-swamp sediments that provide upper limits only. The comparisons in Fig. 9b indicate that the predicted levels lie systematically above the observed limits. At this site, the predicted levels can be lowered by increasing the lithospheric thickness (Fig. 10c), unlike for the Carmel coast where the dependence of the predicted values on H_1 is much less. An increase in lower-mantle viscosity also results in a lowering of the prediction but the dependence on this parameter decreases with increasing viscosity beyond the range considered. Within the range of upper-mantle viscosity used, the amplitudes of the predicted sea level decrease with decreasing viscosity but beyond this range they again increase, and modifications of the earth-model parameters do not bring the observations and predictions into near congruence.

5.3. Versilia plain, Italy

A 70 m core from the Versilia plain of northern Tuscany yield a quite complete Holocene sea-level record (Antonioli et al., 1999b) and sea-level indicators from ~6 to 7 ka BP are 4–9 m below present level. The predicted values here also lie above the observed values, including the continental indicators that specify upper limits only. Lithospheric dependence here is small but of the opposite trend to that for the previous two sites and to force agreement between observations and predictions through modification of the earth rheology requires an increase in either (or both) the upper- or lower-mantle viscosity (Fig. 9b), although the former is inconsistent with the inference from the Carmel coast or from Peloponnisos.

5.4. Côte d'Azur, France

Perhaps the best Late Holocene record from this locality is that inferred from the fossil vermetid and coralline algae record (Laborel et al., 1994) which indicates that at ~4 ^{14}C ka BP levels were about 1.5 m lower than today, and that from at least this time onwards, sea level rose nearly uniformly to its present level. Vertical tectonic movement appears to be negligible on the time scale of concern here (Dubar et al., 1992). The predicted Holocene values agree well with the observed values and no modification of earth-model parameters appears warranted. The earth-model dependence here is similar to that for Versilia and any change in earth-model parameters that may be suggested by the latter data would degrade the agreement with the observed record for the past ~3000 years.

5.5. Ice-load dependence

Across the region, increasing the ice loads over Europe and/or North America has the effect of lowering the sea-level predictions during the Late Holocene interval. Examples are illustrated in Fig. 11 for predictions along the Carmel coast and the Côte d'Azur, two sites where the dependence on ice thickness is, respectively, least and greatest. In these examples, the predictions for the preferred ice models for the two northern regions (NE-2 and NA-2) (i) are compared with model predictions in which (ii) NE-2 is replaced by NE-1 only, (iii) NA2 is replaced by NA-1 only, and (iv) both NE-2 and NA-2 are replaced by the larger-volume ice loads of NE-1 and NA-1, respectively. At the Carmel coast, changes in predictions during the Late Holocene remain small, <1 m at 6 ka BP, and insufficient to change the general observation that the predictions are systematically higher than the observed values. At the Côte d'Azur site, the sensitivity of the prediction on ice load is larger, consistent with the site occurring closer to the ice loads, and reaches ~2 m at 6 ka BP for the modification of both ice sheets but here we see a potential for trade-off between lower-mantle viscosity and ice thickness (compare Figs. 9d and 11b): increasing ice thickness or increasing lower-mantle viscosity lower the Late Holocene predictions at this site. However, modifications of the ice sheets that lead to an substantial increase in ice volume during the LGM and Late Glacial intervals are inconsistent with the outcomes of inversions of the rebound data from the areas of former glaciation.

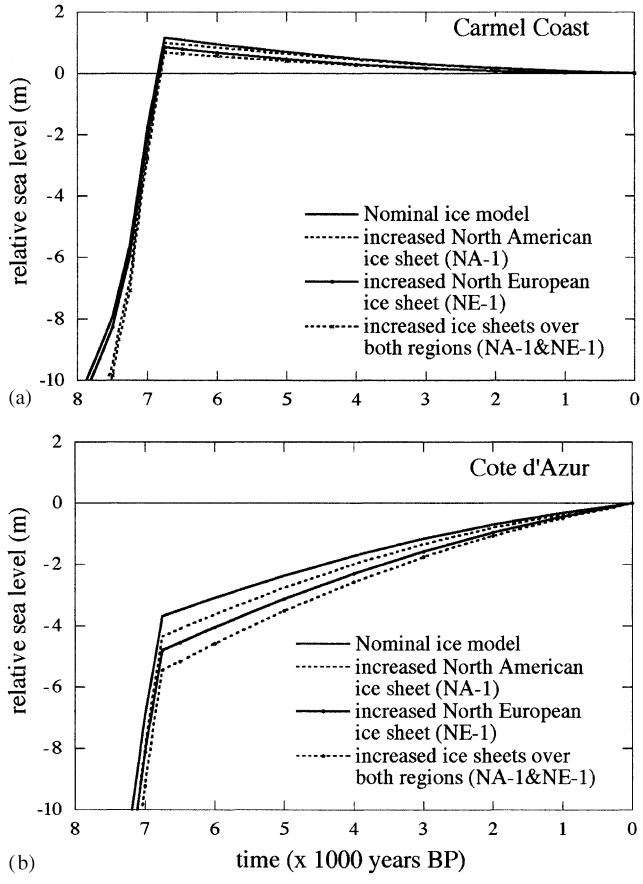

Fig. 11. Predicted sea levels, at (a) the Carmel coast and (b) the Côte d'Azur, for the nominal earth models and different combinations of the two principal northern hemisphere ice sheets. The Antarctic and Alpine contributions are the same in all cases.

5.6. Modification of the esl function

What the preliminary analysis indicates is that with $\Delta\zeta_{esl} = 0$ for $t < 6.8$ ka no choice of earth parameters satisfies all the observational data sets. The modifications required for the sites in the eastern Mediterranean (Carmel coast and Peloponnisos) are at least partly orthogonal to those required for the western Mediterranean sites (Versilia Plain and Côte d'Azur). The alternative solution is to attribute the discrepancies between observations and predictions noted above to inadequacies of the esl function following the analysis suggested by Eq. (5). The data discussed above is inadequate to make precise estimates of the corrections to this function as well as of the rheological parameters but the trend is consistent with analyses carried out for other areas with the esl at ~6.5 ka some 2–3 m less than today and reaching the present-day levels at about 3000 years ago. This esl function (Fig. 12) implies that the total ocean volume did not reach its present value until about 3000 years ago and that between ~7000 and ~3000 BP the ocean volume increased such as to raise the global level by 2.5–3 m (Lambeck, 2002). Whether this is from melting of mountain glaciers or from Antarctic melting, or whether it includes a thermal expansion component cannot be established from this kind of analysis alone, but improved analyses of the

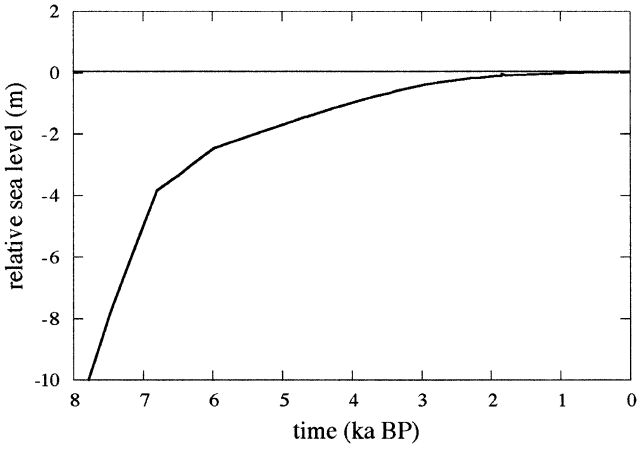

Fig. 12. The global ice volume equivalent sea-level function for the Late Holocene period (from Lambeck, 2002).

Mediterranean sea-level information will lead to improved constraints on fluctuations in ocean volume during the Late Holocene interval.

6. Conclusions

The predicted sea levels at the four test sites are compared with the observed evidence in Fig. 13 in which the predicted values are based on the nominal earth- and ice-model parameters and on the global esl function illustrated in Fig. 12. Agreement between the two is now satisfactory at the Carmel coast, at the Peloponnisos sites and at Versilia plain site, but for the Côte d'Azur the observations lie at the upper limit of the predicted range. Possibly, the global esl function reached its present value

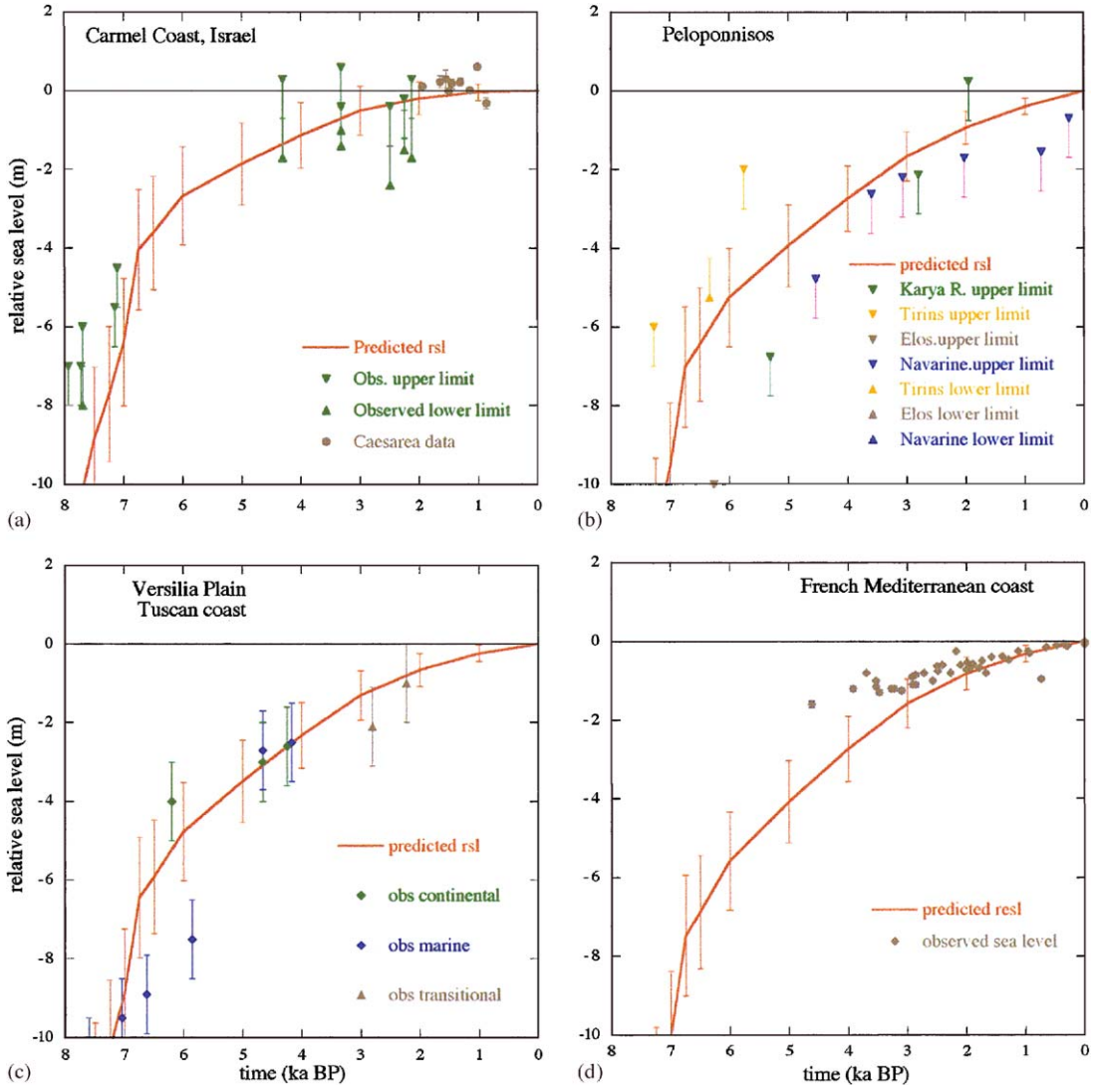

Fig. 13. Comparison of observed and predicted sea levels at four sites with the latter based on the nominal model parameters (E2, NE-2, NA-2), Antarctic and Alpine glacier histories and the modified Late Holocene esl function. The precision of the predicted values are calculated as for Fig. 7b.

earlier than inferred from the far-field data or, because this location is sensitive to the choice of model parameters (c.f. Figs. 8 and 10), the values for the mantle viscosities should be decreased by a small amount. However, until the analyses of a larger Mediterranean data set is completed, and because the global esl model is consistent with data from outside the Mediterranean, we adopt the global estimate for the esl function.

The resulting sea-level predictions are illustrated in Fig. 4 for the LGM, the earliest Holocene, and for the two Late Holocene epochs. An essential characteristic of the predictions is that—in the absence of tectonics—well-developed highstands do not occur at any time within the Mediterranean basin because of the competing effects of the two isostatic contributions $\Delta\zeta_{\text{I-g}}$ and $\Delta\zeta_{\text{I-h}}$ and because of the small ocean volume increase between ~7 and 3 ka BP introduced by the esl correction. These predictions are model-parameter sensitive and while the nominal values adopted give a good first-order description of the observed change, there is potential for parameter improvements using field data from the region. The analysis presented here provides guidelines as to the ideal locations for such data.

Across the region for each epoch, there are locations where the isostatic corrections vanish (see Figs. 2d–f), where the relative sea level equals the equivalent value. Observations from these sites provide the means to effect a direct separation of the isostatic and ocean-volume signals. At other locations, the predictions are insensitive to some of the earth-model parameters, particularly to H_1 and η_{um}, or to both of these parameters (Fig. 8). Other important locations include the north coast of Africa, particularly between and including the Gulfs of Sirte and Gabès, and the coast of Tunisia. Other potentially useful sites include some of the small (e.g. Malta and Lampedusa) or intermediate (e.g. Sardinia) sized islands.

The predictions for 2000 years ago (Fig. 14d) are of particular interest because of the substantial amount of archaeological sea-level markers available for this period (e.g. Flemming, 1969). This includes the tidally controlled piscinae or fish tanks constructed between about 100 BC and 100 AD (Schmiedt, 1972). The model predictions exhibit a spatial variability of ~1 m at this time between sites in North Africa, Italy, and France where Roman period constructions provide sea-level information (e.g. Flemming, 1969; Caputo and Pieri, 1976; Pirazolli, 1976; Morhange et al., 1996) which, where the markers bear a precise relation to the mean level, can provide precise constraints on the predictive model (Lambeck et al., 2004b). Alternatively, comparisons of the model predictions with the archaeological

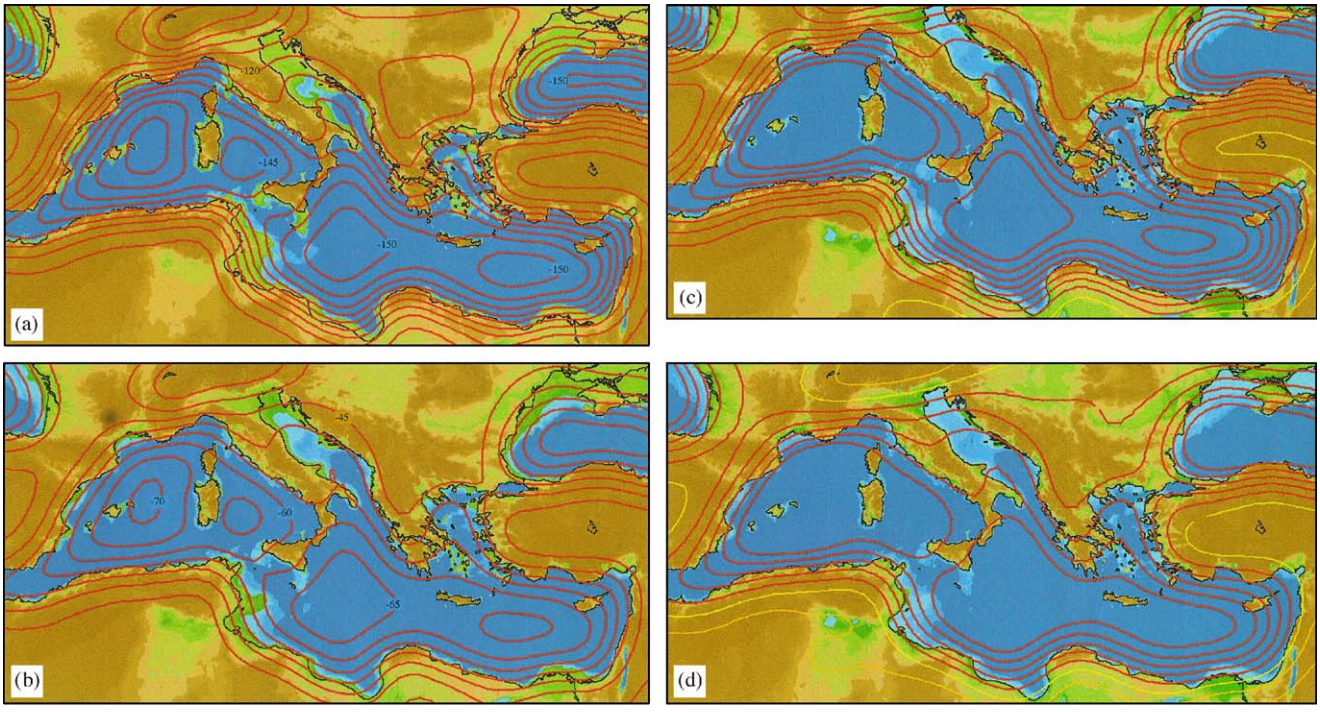

Fig. 14. Predicted relative sea levels and shorelines across the Mediterranean region at four epochs: (a) 20 ka, (b) 12 ka, (c) 6 ka, (d) 2 ka. The palaeo-shoreline positions are defined by the green–blue transition. For 20 and 12 ka BP, the contour intervals are 5 m. For 6 and 2 ka BP, the red contours denote negative values, the orange contours denote positive values, and the yellow contour corresponds to zero change. The contour intervals are 1 m at 6 ka and 0.25 m at 2 ka. The predictions are based on the nominal model parameters (E2, NE-2, NA-2), Antarctic and Alpine deglaciation with on-going deglaciation of the former defined by the esl function for the Late Holocene period (Fig. 12).

evidence may establish the relationship between the structural features.

Throughout the analysis only the glacio-hydro-isostatic signal has been considered and tectonic contributions have been assumed to be either absent or corrected for. The indicator of long-term vertical stability is the elevation of the MIS 5.5 shoreline that, in the Mediterranean, occurs typically between 3 and 10 m above present, at sites where the geological and seismic evidence points to stability (e.g. Carobene and Pasini, 1982; Hearty and Dai Pra, 1986; Antonioli et al., 1999a). Spatial variability in this highstand elevation can be expected across the region, even in the absence of tectonics, because of the isostatic adjustments associated with the ice load fluctuations during the glacial cycle (see the analogous case for the USA Atlantic coast and Caribbean (Potter and Lambeck, 2003) but the evaluation of this for the Mediterranean still remains to be done. Thus, for the present, we assume long-term tectonic stability if these shorelines occur within the above range. This translates into uncertainties in long-term uplift rates, considering a formation age of 124 ± 5 ka for the MIS 5.5 shoreline, of the order 0.3 mm/year and the contribution to the uncertainties in Holocene sea-level inferences remain small, of the order 0.3–0.4 m at 12 ka BP or about 0.5–0.6 m at the LGM.

For a known present-day topography, the palaeo-shorelines and palaeo-water depths can be evaluated using relation (3). Results based on the nominal model parameters used here have been published for the central Mediterranean from the LGM to the present (Lambeck et al., 2004a), and Fig. 14 gives result for 20 and 12 ka BP. The bathymetry used is not of high enough resolution for this result to reveal the fine structure that exists in detailed reconstructions for smaller areas where higher resolution is available. But the result does point to areas where observational information on palaeo-shoreline location would provide important constraints on the predictive model. For example, accurate observations of the LGM sea levels across the broad and shallow Golfe du Lion or North Adriatic Sea would provide useful information, as would the small isolation basins—or near-isolation basins—in the central Adriatic Sea.

References

Antonioli, R., Girotti, O., Improta, S., Nisi, M.F., Puglisi, C., Verrubbi, V., 1999a. New data on Holocene marine transgression and subsidence on Versilian plain by a 90 m core. Le Pianure, Conoscenza e Salvaguardia, Regione Emilia Romagna Ed., pp. 214–218.

Antonioli, F., Silenzi, S., Vittori, E., Villani, C., 1999b. Sea level changes and tectonic stability: precise measurements in 3 coastlines of Italy considered stable during last 125 ky. Physical Chemistry of the Earth 24, 337–342.

Bard, E., Hamelin, B., Fairbanks, R.G., Zindler, A., 1990. Calibration of the ^{14}C timescale over the past 30,000 years using mass spectrometric U-Th ages from Barbados corals. Nature 3455, 405–410.

Caputo, M., Pieri, L., 1976. Eustatic variation in the last 2000 years in the Mediterranean. Journal of Geophysical Research 81, 5787–5790.

Carobene, L., Pasini, G., 1982. Contributo alla conoscenza del Pleistocene superiore e dell'Olocene del Golfo di Orosei (Sardegna orientale). Bollettino della Societa Adriatica di Scienze Trieste 64, 536.

Cathles, L.M., 1975. The Viscosity of the Earth's Mantle. Princeton University Press, Princeton, NJ, pp. 386.

Chappell, J., Shackleton, N.J., 1986. Oxygen isotopes and sea level. Nature 324, 137–140.

Denton, G.H., Hughes, T.J. (Eds.), 1981. The Last Great Ice Sheets. Wiley, New York, 484pp.

Dubar, M., Guglielmi, Y., Falguères, C., 1992. Néotectonique et sédimentation côtie're quaternaires en bordure de l'Arc Subalpin de Nice (A.M., France). Quaternairé 3, 105–110.

Fleming, K., Lambeck, K., 2004. Constraints on the Greenland ice sheet since the Last Glacial Maximum from observations of sea-level change and glacial-rebound modeling. Quaternary Science Reviews 23, 1053–1077.

Flemming, N.C., 1969. Archaeological evidence for eustatic changes of sea level and earth movements in the Western Mediterranean in the last 2000 years. Geological Society of America, Special Paper 109, 1–125.

Galili, E., Nir, Y., 1993. The submerged pre-pottery Neolithic water well of Atlit-Yam, northern Israel, and its palaeoenvironmental implications. The Holocene 3 (3), 265–270.

Galili, E., Weinstein-Evron, M., Ronen, A., 1988. Holocene sea-level changes based on submerged archaeological sites off the northern Carmel Coast in Israel. Quaternary Research 29, 36–42.

Hanebuth, T., Stattegger, K., Grootes, P.M., 2000. Rapid flooding of the Sunda Shelf: a late-glacial sea-level record. Science 288, 1033–1035.

Hearty, P.J., Dai Pra, G., 1986. Aminostratigraphy of quaternary marine deposits in the Lazio Region of central Italy. Zeitschrift für Geomorphologie, Supplementband 62, 131–140.

Johnston, P., 1993. The effect of spatially non-uniform water loads on the prediction of sea-level change. Geophysical Journal International 114, 615–634.

Johnston, P., 1995. The role of hydro-isostasy for Holocene sea-level changes in the British Isles. Marine Geology 124, 61–70.

Johnston, P., Lambeck, K., Wolf, D., 1997. Material versus isobaric internal boundaries in the Earth and their influence on postglacial rebound. Geophysical Journal International 129, 252–268.

Kaufmann, G., Lambeck, K., 2002. Glacial isostatic adjustment and the radial viscosity profile from inverse modeling. Journal of Geophysical Research 107, ETG5-1–ETG5-15.

Kelletat, D., Kowalczyk, G., Schröder, B., Winter, K.-P., 1976. A synoptic view on the neotectonic development of the Peloponnesian coastal regions. Zeitschrift der Deutschen Geologischen Gesellschaft (Journal) 127, 447–465.

Kraft, J.C., Rapp, J.G.R., 1975. Late Holocene palaeogeography of the coastal plain of the Gulf of Messenia, Greece, and its relationships to archaeological settings and coastal change. Geological Society of America Bulletin 86, 1191–1208.

Kraft, J.C., Rapp, J.G.R., Aschenbrenner, S.E., 1980. Late Holocene palaeogeomorphic reconstructions in the area of the Bay of Navarino: Sandy Pylos. Journal of Archaeological Science 7, 187–210.

Kraft, J.C., Aschenbrenner, S.E., Rapp, G.J., 1997. Palaeogeographic reconstructions of coastal Aegean archaeological sites. Science 195, 941–947.

Laborel, J., Morhange, C., Lafont, R., Le Campion, J., Laborel-Deguen, R., Sartoretto, S., 1994. Biological evidence of sea-level rise during the last 4500 years on the rocky coasts of continental southwestern France and Corsica. Marine Geology 120, 203–223.

Lambeck, K., 1993. Glacial rebound of the British Isles—II. A high resolution, high-precision model. Geophysical Journal International 115, 960–990.

Lambeck, K., 1995a. Constraints on the Late Weichselian ice sheet over the Barents Sea from observations of raised shorelines. Quaternary Science Reviews 14, 1–16.

Lambeck, K., 1995b. Late Pleistocene and Holocene sea-level change in Greece and south-western Turkey: a separation of eustatic, isostatic and tectonic contributions. Geophysical Journal International 122, 1022–1044.

Lambeck, K., 1996. Sea-level change and shoreline evolution in Aegean Greece since Upper Palaeolithic time. Antiquity 70, 588–611.

Lambeck, K., 2002. Sea-level change from mid-Holocene to recent time: an Australian example with global implications. In: Mitrovica, J.X., Vermeersen, B. (Eds.), Glacial Isostatic Adjustment and the Earth System. American Geophysical Union, Washington, DC, pp. 33–50.

Lambeck, K., Bard, E., 2000. Sea-level change along the French Mediterranean coast since the time of the Last Glacial Maximum. Earth and Planetary Science Letters 175, 203–222.

Lambeck, K., Chappell, J., 2001. Sea level change through the last Glacial Cycle. Science 292, 679–686.

Lambeck, K., Johnston, P., 1998. The viscosity of the mantle: evidence from analyses of glacial rebound phenomena. In: Jackson, I. (Ed.), The Earth's Mantle: Composition, Structure, and Evolution. Cambridge University Press, Cambridge, pp. 461–502.

Lambeck, K., Nakada, M., 1990. Late Pleistocene and Holocene sea-level change along the Australian coast. Palaeogeography, Palaeoclimatology, Palaeoecology (Global and Planetary Change Section) 89, 143–176.

Lambeck, K., Purcell, A., 2003. Glacial rebound and crustal stress in Finland. Technical Report 2003-10 Posiva Oy, Olkiluoto, Finland.

Lambeck, K., Smither, C., Johnston, P., 1998. Sea-level change, glacial rebound and mantle viscosity for northern Europe. Geophysical Journal International 134, 102–144.

Lambeck, K., Yokoyama, Y., Johnston, P., Purcell, A., 2000. Global ice volumes at the Last Glacial Maximum. Earth and Planetary Science Letters 181, 513–527.

Lambeck, K., Yokoyama, Y., Purcell, A., 2002. Into and out of the Last Glacial Maximum sea level change during oxygen isotope stages 3–2. Quaternary Science Reviews 21, 343–360.

Lambeck, K., Purcell, A., Johnston, P., Nakada, M., Yokoyama, Y., 2003. Water-load definition in the glacio-hydro-isostatic sea-level equation. Quaternary Science Reviews 22, 309–318.

Lambeck, K., Antonioli, F., Purcell, A., Silenzi, S., 2004a. Sea-level change along the Italian coast for the past 10,000 yr. Quaternary Science Reviews 23, 1567–1598.

Lambeck, K., Anzidei, M., Antonioli, F., Benini, A., Esposito, A., 2004b. Sea level in Roman time in the Central Mediterranean and implications for recent change. Earth and Planetary Science Letters 224, 463–575.

Licciardi, J.M., Clark, P.U., Jenson, J.W., Macayeal, D.R., 1998. Deglaciation of a soft-bedded Laurentide ice sheet. Quaternary Science Reviews 17, 427–448.

Meier, M.F., 1993. Ice, climate and sea level: do we know what is happening? In: Peltier, W.R. (Ed.), Ice in the Climate System. NATO ASI Series I. Springer, Heidelberg, pp. 141–160.

Milne, G.A., 1998. Refining models of the glacial isostatic adjustment process. Ph.D. Thesis, University of Toronto, Toronto, Canada.

Milne, G.A., Mitrovica, J.X., 1998. Postglacial sea-level change on a rotating earth. Geophysical Journal International 133, 1–19.

Milne, G.A., Davis, C.H., Mitrovica, J.X., Scherneck, H.-G., Johansson, J.M., Vermeer, M., Kolvula, H., 2001. Space-geodetic constraints on glacial isostatic adjustment in Fennoscandia. Science 291, 2381–2385.

Mitrovica, J.X., 1996. Haskell [1935] revisited. Journal of Geophysical Research 101, 555–569.

Mitrovica, J.X., 2003. Recent controversies in predicting post-glacial sea-level change: a viewpoint. Quaternary Science Reviews 22, 127–133.

Mitrovica, J.X., Forte, A.M., 1997. Radial profile of mantle viscosity: results from the joint inversion of convection and postglacial rebound observables. Journal of Geophysical Research 102, 2751–2769.

Mitrovica, J.X., Milne, G.A., 2003. On post-glacial sea level: I. General theory. Geophysical Journal International 154, 253–267.

Morhange, C., Laborel, J., Hesnard, A., Prone, A., 1996. Variation of relative mean sea level during the last 4000 years on the northern shores of Lacydon, the ancient harbour of Marseille (Chantier J. Verne). Journal of Coastal Research 12 (4), 841–849.

Nakada, M., Lambeck, K., 1987. Glacial rebound and relative sea-level variations: a new appraisal. Geophysical Journal of the Royal Astronomical Society 90, 171–224.

Nakiboglu, S.M., Lambeck, K., Aharon, P., 1983. Postglacial sea levels in the Pacific: implications with respect to deglaciation regime and local tectonics. Tectonophysics 91, 335–358.

Oerlemans, J., 1999. Comments on "Mass balance of glaciers other than the ice sheets", by J. Graham Cogley and W.P. Adams. Journal of Glaciology 45, 397–398.

Peltier, W.R., 2002. Comments on the paper of Yokoyama et al. (2000), entitled Timing of the Last Glacial Maximum from observed sea level minima. Quaternary Science Reviews 21, 409–414.

Peltier, W.R., Andrews, J.T., 1976. Glacial-isostatic adjustment—1. The forward problem. Geophysical Journal of the Royal Astronomical Society 46, 605–646.

Pirazzoli, P.A., 1976. Sea level variations in the northwest Mediterranean during Roman times. Science 194, 519–521.

Potter, E.-K., Lambeck, K., 2003. Reconciliation of sea-level observations in the western North Atlantic during the last glacial cycle. Earth and Planetary Science Letters 217, 171–181.

Schmiedt, G., 1972. Il livello antico del mar Tirrento. In: Olschki, E. (Ed.), Testimonianze da resti archeologici. Firenze, 323pp.

Sivan, D., Lambeck, K., Galili, E., Raban, A., 2001. Holocene sea-level changes along the Mediterranean coast of Israel, based on archaeological observations and numerical model. Palaeogeography, Palaeoclimatology, Palaeoecology 167, 101–117.

Sivan, D., Lambeck, K., Toueg, R., Raban, A., Porath, Y., Shirman, B., 2004. Ancient coastal wells of Caesarea Maritima, Israel, an indicator for sea level changes during the last 2000 years. Earth and Planetary Science Letters 222, 315–330.

Stone, J., Balco, G.A., Sugden, D.E., Caffee, M.W., Sass, L.C., Cowdery, S., Siddoway, C., 2003. Holocene deglaciation of Marie Byrd Land, West Antarctica. Science 299, 99–102.

Tromp, J., Mitrovica, J.X., 1999a. Surface loading of a viscoelastic earth—I. General theory. Geophysical Journal International 137, 847–855.

Tromp, J., Mitrovica, J.X., 1999b. Surface loading of a viscoelastic earth—II. Spherical models. Geophysical Journal International 137, 856–872.

Tushingham, A.M., Peltier, W.R., 1992. Validation of the ICE-3G model of Würm–Wisconsin deglaciation using a global data base of relative sea level histories. Journal of Geophysics Research 97, 3285–3304.

van Andel, T.H., 1987. The adjacent sea. In: van Andel, T.H., Sutton, S.B. (Eds.), Landscape and People of the Franchthi Region. University Press, Bloomington, pp. 31–54.

Yokoyama, Y., Lambeck, K., De Deckker, P., Johnston, P., Fifield, L.K., 2000. Timing of the Last Glacial Maximum from observed sea-level minima. Nature 406, 713–716.